Radiance Covariance and Climate Models

Robert Haskins[1], Richard Goody[2], and Luke Chen

Jet Propulsion Laboratory

California Institute of Technology

Pasadena, CA. 91109

Submitted to *Journal of Climate*

[1] Robert Haskins died while this paper was in review. Bob was an important figure in the remote sensing program at JPL. This work was a sideline, but he was very proud of it. R.G., L.C.

[2] Corresponding author: 101 Cumloden Drive, Falmouth, MA 02541-0430. Telephone (508)540-4437, email rgoody@capecod.net.

Abstract

Spectral Empirical Orthogonal Functions (EOFs) derived from the covariance of satellite radiance spectra may be interpreted in terms of the vertical distribution of the covariance of temperature, water vapor, and clouds. This has been done for four major geographic regions: the tropical oceans; mid-latitude oceans; and three important land areas. The purpose of the investigation is to demonstrate the important constraints that resolved spectral radiances can place upon climate models.

1. Introduction

The need for a comprehensive global climate observing system in order to test the predictions of climate models is often remarked upon in the scientific literature *e.g.*, Gates, *et al.* (1995). In a series of papers we have examined the importance of satellite observations of calibrated, resolved, thermal radiances in this context. Haskins, Goody and Chen (1997), hereafter called HGC, discussed statistical aspects of data from the 1970/71 IRIS mission, including spectral Empirical Orthogonal Functions (EOFs), and showed how modeled and observed statistics could be compared. Goody and Haskins (1998) showed that resolved radiances provide very high precision, absolute data..

Satellite measurements of spectrally resolved thermal radiances have a unique status for climate observing. They give direct information on the planet's attempts to reach energy balance, the most fundamental of all constraints upon climate. Because they can be calibrated against absolute standards they can be compared directly to other, independent radiance measurements. They provide homogeneous data over most or all of the globe, and they carry information on the vertical profiles of the essential climate variables; temperature, water vapor and cloud. They give quantitative and interpretable thermodynamic information on clouds, perhaps the most important, and least understood, element in the internal variability of the atmosphere.

The questions remaining relate to the interpretation of the data. The purpose of this paper is to take the discussion of resolved spectral radiances a step further by inverting second-order spectral statistics (specifically Empirical Orthogonal Functions or EOFs) to give covariances of temperature, humidity and cloud in the troposphere and lower stratosphere so that the constraints imposed upon climate models by radiance data are in a form more familiar to climatologists.

a. The use of second-order statistics

The comparison between mean values of atmospheric parameters as given by a general circulation model (GCM) and as currently observed has been a major part of attempts to assess the value of climate models (Gates, *et al.*, 1996). It is important for a GCM to reproduce correctly the current mean climate but good agreement gives no reason to believe predictions of perturbed climate states. According to Leith (1975) the important comparison is between time-lagged covariances among climate variables.

Leith applied the fluctuation-dissipation theorem of statistical mechanics to an equilibrium system, with the following results, which will be stated without proof. Consider a system with N independent variables, $u_\alpha(t)$; $\alpha = 1,\dots,N$ satisfying a Liouville equation. Natural variability will cause the variables to fluctuate. The time-lagged covariance matrix is:

$$U_{\alpha\beta}(\tau) = \overline{u_\alpha(t)u_\beta(t-\tau)} \;, \tag{1}$$

where the overbar denotes an ensemble average.

If the system is subjected to a constant, infinitesimal forcing that causes variables to change at rates, $\delta\dot{u}_\beta$, it may be shown that the change of another variable can be stated in the form,

$$\delta u_\alpha = \sum_\beta \int_{-\infty}^{t} g_{a\beta}(\tau)\delta\dot{u}_\beta d\tau, \tag{2}$$

where $g_{\alpha\beta}(\tau)$ is the mean linear response function for the system for the time interval τ. $g_{\alpha\beta}(\tau)$ defines the model's climate sensitivity.

The fluctuation-dissipation theorem states that,

$$g_{\alpha\beta}(\tau) = \frac{U_{\alpha\beta}(\tau)}{U_{\beta\beta}(0)} . \tag{3}$$

The denominator is the total variance of the unperturbed state.

Equation (3) relates the system response function to covariances between climate variables in the unperturbed system; mean values of the variables do not appear in the equation. If the system is to respond correctly, these covariances should be correctly represented and, since they are relatively easy to measure, they provide an attractive basis for model tests. The predictive capability of a model can therefore be tested from statistical data on the unforced system. This is the basis for investigations by Polyak (1996), and by Polyak and North (1997a,b). The validity of equation (3) for real systems has been assessed analytically by Bell (1980) and numerically by North, Bell and Harding (1993). However, the precision of equation (3) is not the issue. The relationship is important because it indicates the critical observations to make; a similar conclusion was reached by HGC on the basis of qualitative reasoning.

This paper does not treat the data in precisely the way suggested by equation (3) in two respects. The first is that the quantities derived from the observed data are not covariances for a single time lag, but are weighted averages over a range of time lags. The data are averaged over 1, 2, 5, or 15 days, and covariances are calculated for all data in a 10-month period. Most commonly 5-day averages are employed, when the result is a weighted average of equation (1) from 5 to 300 days. The second respect is that Empirical Orthogonal Functions (EOFs) are used. EOFs and covariance matrices are two aspects of the same data. Both of these are matters of convenience and presentation; neither affects the information content of the treatment. In this paper it is not our intention to apply equation (3) to derive climate sensitivity, but to verify that basic model physics is realistic by comparing second-order statistics of climate variables for a model with those that are observed.

The restriction to 10 months of data means that only those processes with characteristic times less than 10 months can contribute. Oceanic phenomena, even ENSO, are not involved. However, all time constants intrinsic to the atmosphere as an isolated system are much less than a year, and it is possible to test them with data covering one seasonal cycle. While this may treat only a part of the climate change problem, it is a very important part. A frequently asked public policy question is: How will the atmosphere react if greenhouse gases are doubled, *and no other forcing takes place*? This question can be answered on the basis of a model with correct response on an annual time scale and less.

b. The IRIS data

The IRIS data were gathered over a 10-month period from April 1970 to January 1971. 720 IRIS frequency channels cover the spectral range 400 to 1600 cm^{-1}. Radiances are measured in units of ($mW\ m^{-2}$ $wavenumber^{-1}$ $steradian^{-1}$) which, being cumbersome, will often be omitted. The spectral resolution was 2.8 cm^{-1} and all measurements were in the nadir. The radiometric accuracy was probably better than 1 K, but since variances and covariances are based on differences between two radiance measurements, radiometric accuracy is irrelevant to first order. These data were assembled into 1-, 2-, 5- and 15-day averages for the geographic regions defined in table 1 and figure 1. 5-day averages give the best combination of even sampling and a sufficient number of independent observations, and are most commonly used in this paper.

During the lifetime of the IRIS mission, thousands of individual spectra were recorded in each geographic region, each with a footprint of about 100 km. Figure 2 shows the distribution of individual footprints for one 5-day period in the Central Pacific region, superimposed upon the grid used by the GCM that will be discussed. Both the satellite and the GCM give data at two times of day, approximately 12 hours apart. Equal amounts of data for the two times are averaged to reduce diurnal sampling errors.

Figures from 4 onward show spectra that are derived from IRIS data. Different spectral regions are related to different sources of variability. As discussed in HGC, there are qualitative differences between the following: the two water bands at 400 to 600 cm^{-1} and 1200 to 1400 cm^{-1}; the carbon dioxide fundamental from 600 to 800 cm^{-1}; the window region, 800 to 1200 cm^{-1}; the 1042 cm^{-1} ozone band; and the Q-branch of the fundamental band of methane at 1311 cm^{-1}.

For clear-sky radiances, these spectral bands convey the following information. The methane and water bands refer to the upper- to mid-troposphere. The window region is governed by conditions at and near to the surface. The center and parts of the wings of the carbon dioxide band refer to conditions in the stratosphere, with the center of the principal Q-branch radiating to space from an altitude of 30 km. The ozone band is formed partly in the troposphere and partly in the stratosphere. Ozone concentrations are variable and the GCM that we discuss makes no attempt to model them. The spectral region from 981.0 to 1074.9 cm^{-1} is, therefore, omitted from all inversions. The spectral region from 1400 to 1600 cm^{-1} is also omitted because the signal-to-noise ratio was low.

The above statements do not apply in the presence of cloud. Where cloud is present, radiation from below the cloud top will normally be completely absorbed, and replaced by something close to black-body emission from the cloud top. In the window region, variability may be caused by the variability of cloud amount or by variability of temperature and humidity at the surface or in the lower atmosphere. For the center of the carbon dioxide fundamental, radiation is from the stratosphere, and is unaffected by cloud.

The EOFs that will be discussed in this paper are *spectral EOFs*, i.e. they are based upon covariances between radiances at different frequencies in the spectrum, $I_\nu(\mathbf{x},t)$. Let

$$I'_\nu(\mathbf{x},t) = I_\nu(\mathbf{x},t) - \bar{I}_\nu, \tag{4}$$

where $\mathbf{x}$ is the position vector, t is time, and the overbar indicates an average over time and all positions in a geographic region. The data may be regarded as a vector in ν-space with 720 components corresponding to the 720 observed frequencies. The EOFs, $\phi_\nu^{(i)}$, are unit vectors in ν-space, and they are derived from the covariance matrix,

$$D_{\nu,\nu'} = \overline{I_\nu(\mathbf{x},t)\, I'_{\nu'}(\mathbf{x},t)}\,, \tag{5}$$

by the relationship,

$$D_{\nu,\nu'}\,\phi_{\nu'}^{(i)} = \lambda^{(i)}\,\phi_\nu^{(i)}\,, \tag{6}$$

where $\lambda^{(i)}$ is the i^{th} eigenvalue. An EOF multiplied by its amplitude is a *Principal Component* or *PC*,

$$PC_\nu^{(i)} = \lambda^{(i)\frac{1}{2}}\,\phi_\nu^{(i)}\,. \tag{7}$$

A Principal Component is a vector in ν-space with the dimensions of radiance.

c. Inversions

The radiance can be expressed in terms of variable atmospheric parameters, temperature, humidity and cloud throughout the atmosphere (ozone is not treated here, and carbon dioxide, methane, and nitrous oxide are considered to be of fixed concentrations; aerosols are neglected in common with almost all GCM calculations, an omission that needs more attention in the future). Numerical methods define these parameters in discrete layers from the surface to ~ 40 km. Let the variables be denoted by p_n, and their departures from a space-time mean by p'_n. For small departures from means,

$$I'_\nu = \sum_n \frac{\partial \bar{I}_\nu}{\partial p_n} p'_n , \tag{8}$$

or, in matrix notation,

$$\mathbf{I}' = \mathbf{J}\,\mathbf{p}', \tag{9}$$

where $\mathbf{p}'$ and $\mathbf{I}'$ are vectors whose elements are p'_n and I'_ν, respectively, and **J** is a Jacobian matrix whose elements are $J_{\nu,n} = \dfrac{\partial \bar{I}_\nu}{\partial p_n}$.

The Principal Components are vectors in ν-space that are functions of the departures of radiances from mean values. Each may, therefore, be related to a vector of departures in *p*-space, $\mathbf{E}^{(i)}$, by equation (9),

$$\mathbf{PC}^{(i)} = \mathbf{J}\,\mathbf{E}^{(i)}. \tag{10}$$

There is an extensive literature dealing with the inversion of equation (10), in order that atmospheric parameters may be retrieved from satellite data for weather forecasting purposes. The technique that we have adopted (SR/SVD) is described in the Appendix. In principle, the inversion can yield as many atmospheric parameters as there are frequencies in the spectrum (720), but the inversion is not well-conditioned and many of the elements of the Jacobian are effectively zero, with the result that we recover 19 or less variable atmospheric parameters.

The remainder of this paper is concerned with elements of $\mathbf{E}^{(i)}$, i.e. departures of atmospheric parameters from space-time means. Since a Principal Component represents data that are correlated between frequencies, the recovered p'_n s are the correlated departures from their means that give rise to the Principal Component. It does not, however, follow that $\mathbf{E}^{(i)}$, is a Principal Component of the variable atmospheric parameters.

It is appropriate here to remind the reader of a statement made in §1, that the purpose of this discussion is to demonstrate "the constraints imposed on climate models [*by spectral statistics*] in a form familiar to climatologists". Data inversions, as described here, may not be the best approach to utilization of radiance data for testing climate models. We return to this subject in §5.

The elements of the Jacobian are calculated from differences between two spectra, one calculated before and one after a change of a parameter by a given amount in a given layer. The layers and parameters used are: *relative humidity (percent)*, W2 (0-2 km), W4 (2-4 km), W6 (4-6 km), W8 (6-8 km), W12 (8-12 km), W16 (12-16 km); *temperature (kelvin)*, T0 (ground temperature), T2 (0-2 km), T4 (2-4 km), T6 (4-6 km), T8 (6-8 km), T12 (8-12 km), T16 (12-16 km), T30 (20-30 km), T40 (30-40 km); *clouds (fraction)*, C4, C8, C12, C16, opaque cloud tops at 4, 8, 12 and 16 km, respectively.

Radiances contributions were calculated by the medium-resolution program MODTRAN (Kneizys, *et al.*, 1988, Wang, *et al.*, 1996, and Bernstein *et al.*, 1996). A (1-2-1) running average over 1 cm^{-1} intervals gives a spectral transfer function similar to IRIS. Because two spectra are subtracted when forming variances and covariances most errors in MODTRAN should have little effect on the final result. In one instance, however, MODTRAN calculations are probably unsatisfactory. The Q-branches of the two hot bands flanking the carbon dioxide fundamental are very sensitive to temperature and the version of MODTRAN used here does not incorporate line mixing. This effect is apparent in Figure 3 in the relatively large departures in the Q-branches at 618 and 721 cm^{-1}. It was rarely possible to match the observed variances in these Q-branches, but that had little overall effect on our results. Four of the calculated difference spectra are shown in figure A1.

Jacobians depend, to some degree, on the atmospheric state of all higher layers. MODTRAN offers alternative standard atmospheres including tropical and mid-latitude summer and winter atmospheres. These three cases give significantly different results. Seasonal change in the tropics is small and use of a single standard atmosphere was judged to be appropriate. Mid-latitudes, on the other hand, should preferably be broken down by season. Since seasonal standard atmospheres were not available, mid-latitude cases using the entire IRIS data set were calculated twice, *both* for summer *and* for winter elements, in order to bracket the uncertainties; both are reported in relevant sections.

Not all contributions to the radiance are both important and independent. W16 was used in the analysis but never contributed significantly to a solution. The elements C8 and C16 can be combined to give a spectrum very similar in shape to C12. Although the distinction among these three cloud layers is preserved in the analysis, they are best regarded as indicating high clouds, with tops somewhere between 8 and 12 km. For less obvious reasons, C4 and T2 are virtually indistinguishable in shape, and a single contribution from C4T2, expressed in kelvin, is employed; C4T2 may be interpreted as either a cloud or a temperature element. Other elements are correlated to lesser degrees. Those which have correlation coefficients in excess of 0.9 are shown in table 2. We may anticipate ambiguities in the interpretation when these elements are involved.

d. Errors and Significance

Given ideal inversions, errors in interpretation should depend only on the significance of the EOFs or upon system noise in the retrieval process (see Rodgers, 1990, for general discussion). EOF significance in the presence of a noisy data field is difficult to establish (Preisendorfer, 1988), but all of our analysis is confined to the first and second EOFs, the significances of which are obvious. Errors due to system noise are negligible because of the large data sets that are used here. The vertical structure used in the analysis is coarse, and it is possible that no combination of contributions can fit the data exactly, giving rise to large null-space errors (see Rodgers, 1990). One aspect of compatibility involves the MODTRAN program, and the approximate procedure used to imitate the IRIS spectral transfer function. Both are inexact and are responsible for most of the departures in figure 3 (a better fit is usually obtained when GCM data are analyzed because these are also generated from MODTRAN). The root-mean-square amplitude of the residual in figure 3 is the *residual rms*. It may be used in a measure of the goodness of fit (*g.o.f.*) of a solution, and can also be used to place a bound on the significance of individual layer contributions. If the root-mean-square amplitude of a Principal Component, is the *PC rms*, the goodness of fit for a solution is defined by,

$$g.o.f. = 100\frac{(\,PC\ rms)^2 - (residual\ rms)^2}{(PC\ rms)^2} \quad . \tag{11}$$

The contribution to a Principal Component by a single variable is one of the terms on the right hand side of equation (9). Its root mean square is *the contribution rms*,

$$contribution\ rms\ = p_n' \left[\sum_{\nu} J_{\nu,n}^{2} \right]^{\frac{1}{2}} \quad . \tag{12}$$

The *contribution rms* is compared to the *residual rms* in figures 7, 8, 9, and 10, and in tables 3, 4, 6, and 8. If the *contribution rms* exceeds the *residual rms* the contribution is considered to be significant. This is a conservative approach, and the opposite conclusion (that a *contribution rms* less than the *residual rms* is not significant) is not necessarily correct. The discussion in subsequent sections is restricted to contributions that are very significant on this criterion.

2. The tropical oceans

In many ways the tropical oceans dominate the climate system. As representative areas we examine the Warm Pool, the Indian Ocean, and the Central Pacific (see table 1 and figure 1 for definitions of the geographical regions). Since sea-surface temperature is warmer over the tropical oceans than in other regions of the globe, it is possible to identify spectra with relatively clear skies (screened data) for these three regions by comparing maximum brightness temperatures in the window region with climatological sea-surface temperatures (see HGC for details of the procedure). The use of the screened data is discussed in §2.b.

Figures 4, 5, and 6 show the average radiances, standard deviations of radiance, PC1 and PC2 from IRIS observations for the Warm Pool, the Central Pacific, and the Indian Ocean, respectively, for both the complete data set and for the screened data.

a. Vertical structure of covariance

The vertical structure of covariance for the tropical Pacific PC1s, as shown in figures 4, 5, and 6 for the complete data set, has been analyzed by the SR/SVD technique (see Appendix). The results are shown in figure 7. In all three regions the cloud gives the major variance contribution, and it is the main reason for the large explained variances for all three PC1s (Warm Pool 98.3%, Central Pacific 93.3%, Indian Ocean 97.9%). However, that is not the whole story. The water and temperature variations shown in figure 7 are correlated with the cloud variations and with each other, and contribute to the explained variance of the PC1.

The significance of the contributions in figure 7 can be judged from contribution and *residual rms*'s, see §1.d. Most contributions are significant. The most significant elements for the individual regions are: Central Pacific, C4T2, W12, W6; Indian Ocean, C4T2, T4, W2; Warm Pool, W8, T6. For all of these the *(contribution rms)/(residual rms)* ratio is at least 3. All contributions may not be independent. From table 2, W2 for the Indian Ocean may be associated with C4T2. For the Warm Pool W8 and T6 may be associated.

The three sets of profiles in figure 7 have both similarities and differences. The water profiles for Indian Ocean and Warm Pool are similar. Since the data are independent, this agreement is unlikely to happen by chance, and confirms the significance that we attribute to the inversions. The water profiles for Central Pacific differ from the others, however; the large value of W12 is highly significant. As far as temperature is concerned, the elements T12 for Central Pacific and Indian Ocean have *(contribution rms)/(residual rms)* ratios of about 1.5. The IRIS Central Pacific clear-sky temperature profile shown in figure 8b is very close to the temperature profile in figure 7a. It is not surprising that a cloudy PC should show a combination of cloud and clear-sky behavior. What is not obvious, however, is why they are correlated.

b. Comparison between IRIS and a GCM

GCM data were not available for the IRIS observing period, and instead comparison is made with a similar phase of ENSO during 1988 (see HGC for details). The GCM data available to us did not include enough data on clouds to permit radiance calculations in the presence of cloud cover. Comparison is, therefore, limited to screened (clear-sky) data obtained in the same manner as HGC. PC1s for screened data in the three tropical Pacific regions, and the SR/SVD analyses are shown in figures. 8, 9, and 10.

Agreement between regions for IRIS is fairly close: the same is true for GCM taken independently. For IRIS water activity, all three regions show W2, W4, W6, W8 (marginally), and W12 (bottom half only shown in the figures), with the same signs. IRIS temperature behavior is dominated by a large negative C4T2 in all three regions. This may be caused by low cloud rather than temperature; the method adopted for screening spectra could miss small amounts of low cloud, and include the spectrum in a clear-sky category. There is also consistency among the GCM results. Water elements W6 and W8 dominate. C4T2 has significant contributions in all three regions, but the contributions are positive in Central Pacific and Indian Ocean but negative in Warm Pool.

Commonality between GCM and IRIS is exhibited by significant contributions from W6 and other tropospheric water, and from temperature activity, principally in the surface layers. But the disagreements are significant. This comparison illustrates the possibility of identifying problem areas for a GCM using radiance data, but until calculations are available at the same time as observations, and until a GCM can provide suitable cloud parameters, such comparisons are of limited value.

3 Mid-latitude oceans

a. Weather and seasonal covariance

Two representative regions have been chosen in the North and South Pacific (see table 1 and figure 1). Although they are geographic mirror images, there are important differences between these two regions and between them and the Central Pacific region. These differences are interestingly illustrated by standard deviation spectra based on 1-day, 2-day, 5-day and 15-day averages (figure 11). The Central Pacific is, for the purposes of this discussion, not very different from the Warm Pool and the Indian ocean, see figures 4, 5, and 6, apart from the scale of the variance (square of the standard deviation).

The representation of the data in figure 11 allows a distinction to be made between "weather" and "seasonal" variance. The 1-day averages should contain most of the weather variance and all of the seasonal variance, while the 15-day averages should contain almost no weather variance but most of the seasonal variance. The difference between the two represents mainly weather variance. Both sources of variance are important for maintaining the climate state.

The general level of cloud activity, as indicated by the magnitude of the standard deviation at 900 cm^{-1}, is not dissimilar in North, South, and Central Pacific, but the time spectrum of North Pacific is unique in showing almost no variance on the time scales between 5 to 15 days. The weather variance in the North Pacific is at higher frequencies than elsewhere in the Pacific. This has an interesting consequence. For North Pacific the seasonal standard deviation is almost twice as large as for South Pacific and Central Pacific, which has an influence on the Principal Components (§3.b).

The most striking feature of the comparison between the tropics and mid-latitudes in figure 11 is the contrast between the variations in the window region (mainly clouds) and variations in the carbon dioxide fundamental (mainly stratospheric). In the Central Pacific the stratosphere is quiescent compared to the cloud, but North and South Pacific, particularly the latter, show large stratospheric variance. Unlike the cloud variance, the stratospheric variance has 1-day and 15-day averages that are almost the same; the stratospheric variance is almost entirely seasonal.

b. The Principal Components and the vertical structure of covariance

The first two Principal Components (PC1 and PC2) are shown in figures 12 and 13 for 1-day and 15-day averages. For 1-day averages the PC1s for both the North and South resemble the Central Pacific (figure 5c), with little contribution from the carbon dioxide band, despite its prominence in the North and South standard deviations. From this we may conclude that the stratospheric and cloud variations are largely uncorrelated. The stratospheric variance appears in the PC2 (figure 13), with almost all of the contributions from the carbon dioxide and ozone bands, and very little contribution from clouds.

The 15-day averages present a different picture. In the North Pacific they resemble the 1-day averages, but they differ greatly in the South Pacific. For the North Pacific, the stratospheric variance is unchanged as the averaging period increases and, while the cloud variance decreases, it does not do so by very much (figure 11a). For the South Pacific, on the other hand, the stratospheric variance is larger, while the cloud variance decreases more rapidly with averaging time. The numbering of the PCs is based on their explained variance, and has no inherent physical significance. For the South Pacific the explained variance for 1-day averages is 71.5% for a mainly 'cloud' PC and 24.9% for a 'stratospheric' PC, while for 15-day averages the figures are reversed in order, 31.2% and 66.2%, respectively.

Table 3 shows the cloud and the next two elements of importance from the SR/SVD analysis. The switch in the order of the PCs in the South Pacific going from 1-day to 15-day averaging is shown explicitly, and the table justifies the qualitative identification of 'cloud PCs' and 'stratospheric PCs' that was made in previous paragraphs. The table also shows orthogonality of stratospheric and tropospheric behavior in the North and South Pacific. Stratospheric and tropospheric elements do not occur together except for a small correlation between C12 and T30 in PC2 of the South Pacific.

4 Three land areas

Land areas differ greatly from one another. We discuss three particularly interesting regions, the Amazon, the Sahara and the Siberian Tundra.

a. Amazon

IRIS data for the Amazon are shown in figure 14. There is a striking similarity to the Warm Pool (figure 4), except that the Amazon variance is much larger (see table 1). The ozone band in PC2 is the only important qualitative difference between the two regions, but the PC2 share of the variance is small for both regions (1.7% for Amazon, 1.1% for Warm Pool).

The reason for this coincidence is that both the Amazon and the Warm Pool are dominated by the presence of a cloud layer, at 16 km for the Amazon and at 12 km for the Warm Pool (the distinction between the two cloud layers is slight). For the Amazon the *PC1 rms* is 5.77, while the *contribution rms* for the single cloud element is 5.62; for the Warm Pool the figures are 3.49 and 3.38, respectively. Table 4 shows the principal elements in the SR/SVD analysis of PC1 for the Amazon.

b. Sahara

Data for the Sahara are shown in table 5 and figure 15. The Sahara shows unusual and interesting features, most of which do not appear to be recorded in existing climatologies. Three points illustrate the variety of phenomena that can be determined quantitatively from observations of resolved variances. First, the radiance (figure 15a) stays remarkably constant during spring, summer and fall, and falls only in the winter season. Second, the total variance (summed over all frequencies) within seasons is very changeable (table 5), with the variance in spring nearly five times that in the winter. Third, the variance behaves in an unusual way with respect to the averaging time (table 5). Little variance is present between 2 and 5 days averaging, but there is significant variance between 5 days and 15 days, suggesting that there are strong disturbances in the Sahara with periods about 10 days. Despite the change of total variance between seasons, the PCs for each season are similar, showing that there is little change in the physical processes between seasons, although the degree of activity changes. SR/SVD analysis on 5-day averages of all IRIS data is given in table 6.

For the Sahara, unlike the tropical regions, high clouds play little part in the variance of the observed radiances, with the result that no single element dominates the PC1. The most important element is T0, the surface temperature. Next is C4T2. The only other activity is W2 but the summer and winter contribution are inconsistent. All of these activities are associated with a dominant convective boundary layer.

c. Siberian Tundra

The Siberian Tundra is the most active region studied, see table 1, and it has other unique features, see figure 16. Little of its large variability is attributable to weather. According to the data in table 7, the total variance between averaging times of 1 and 15 days, which contains all the weather variance and some of the seasonal variance, is 1.6×10^4, while the seasonal (15-day) total variance is 5.5×10^4. Figure 16b gives more details. The stratospheric variance (in the carbon dioxide band) is almost entirely seasonal.

The total variance per season is shown in table 7. The ratio between fall variance and winter variance is remarkably large, a factor of about 13. However, the average total variance within seasons is quite small, 2.0×10^4, which may be contrasted with the total variance for the whole data set (for 5-day averages), 6.28×10^4. For 5-day averages, 69% of the total variance lies between time scales of 90 days (a season) to 300 days (the data set).

Some insight into these long time scales is given by the seasonally averaged radiances, see figure 16a. At 900 cm^{-1}, the difference between summer and winter radiances corresponds to about a 30K change in the lower atmosphere temperature variance.

An unusual feature of figure 16a is that the entire spectrum rises and falls together. For all other cases that we have examined the carbon dioxide band is not, or only to a small degree, covariant with the window region. Thus the characteristic features of surface and stratosphere changes have not, up to now, occurred in the same PC, while PC1 for all Tundra data (figure 16c) shows lower atmosphere features together with a substantial contribution from the stratosphere.

Table 8 shows the principal contributions from an SR/SVD analysis. Contributions are from temperature only, principally from the troposphere, and to a lesser degree from the lower and upper stratosphere. The amplitudes of these contributions are large, approximately 10K, which is consistent with the discussion of seasonally averaged radiances above.

5 Discussion

The variety and precision of information available from second-order statistics of resolved radiances is demonstrated by our results. Matching model predictions to observations for these data can severely test climate model performance; the work of Leith (1975) shows that these are the appropriate tests to ensure that a model has the correct climate sensitivity.

A series of papers by Polyak (1996), Polyak and North (1997a,b) and Kim, North and Hegerl (1996) also deal with climate model tests, and for the same reasons. Polyak and North (1997a,b) compare surface temperatures from the Geophysical Fluid Dynamic Laboratory GCM with observed data. In the first paper they consider univariate and autocorrelation functions of the data; in the second they discuss multivariate (time and latitude) autoregressive and linear regression model parameters and find discrepancies between observations and the GCM. For example, in the tropics the latitude-temporal correlation functions that are observed are larger, and the distribution much broader, than for the GCM. They conclude that these are appropriate means for the "discovery of important errors in the physics or the numerical methodology."

Santer and Wigley (1990) use a more conventional synoptic approach and compare maps of mean values and variances of mean sea-level pressure for three models with observations. They are concerned with the significance of comparisons between maps when the patterns are correlated. Kim, North and Hegerl (1996) avoid this problem by explicit use of the covariance patterns of the surface data (*i.e.*, the two-dimensional EOFs). This is analogous to the procedures of this paper in the spectral domain; the spectral and spatial domains could be combined if that should add significantly to the information content of the data. To judge from the explained variance of the EOFs, the spectral EOFs in this paper give much more specific information than do the surface EOFs of Kim, North and Hegerl. While explained variances for the first EOF of 90% are common in the spectral data, the first five surface EOFs together explain only between 39% and 57%, with the result that there is significant crossing between modes.

This paper interprets satellite radiance covariances in terms of covariance of conventional meteorological data in order to demonstrate the information content in terms familiar to climatologists. Nevertheless, this is probably not the way in which the data should be used for testing climate models. Radiances are now assimilated directly into numerical weather prediction models. Using inverse modeling, based on the adjoint equations (e.g., Derber, 1989; Errico and Vukicevic, 1992), model sensitivity, tuning and stability analysis can be performed. Inverse modeling may be the best procedure for climate models as well. It would yield information on the errors in the physical processes upon which the model is based. As far as we are informed, this has yet to be done for a climate model, but it would be an appropriate step in a systematic approach to model testing.

The importance of clouds in climate is a prominent conclusion from this study. This is scarcely a new idea, but what is new is that the radiance data on cloud variations are *objective* and *quantitative*, and such data have not been previously available for climate research. Variance from clouds dominates most of the cases examined. A model that cannot reproduce these variances and covariances is unlikely to yield quantitative predictions of climate change.

To move beyond this point, and to lead to better climate predictions, requires that a number of things must happen. For the radiation calculations, greater accuracy is required than is given by MODTRAN. More precise line-by-line codes are available but, when combined with multiple scattering calculations, they can use unreasonably large amounts of computing time. Economical calculations need to be developed. In addition to increased accuracy, line-by-line calculations can give higher spectral resolution that is available from MODTRAN, and this will be needed in the future. AIRS and other planned observing systems will have higher resolution than IRIS, and higher than MODTRAN can achieve. This higher resolution should be used to the fullest extent because it offers important increases in the information content of the radiance spectra.

Better data are required from the GCMs. In the first place, calculations simultaneous with the observations are required, but this will certainly be available for future observations. It goes without saying that the GCMs must have good cloud models, but it is also necessary that the data upon which the cloud calculations in the model are based must be available along with normal meteorological variables; this has not been the case before now.

Finally, new observing systems are required. Fortunately, even if specific climate missions are not flown, there is reason to believe that the required spectral data will become available during the next decade. The AIRS spectrometer on the EOS-PM1 mission is primarily designed for weather forecasting, but it can also be used for spectral covariance analysis. A European Fourier transform spectrometer is also in the planning stage. The opportunity is opening up to resolve some of the more vexing problem associated with the reliability of climate predictions by testing models objectively against data.

Acknowledgments

An anonymous reviewer provided valuable comments on the mathematical presentation. Professor Y.L. Yung and Dr. S. Leroy helped us with the necessary corrections, in the absence of Bob Haskins, and we are greatly indebted to them. The research described in this paper was carried out by Jet Propulsion Laboratory, California Institute of Technology, under a contract with the National Aeronautics and Space Administration.

Appendix. Inversion Methodology

Equation (10) must be inverted to obtain the elements, p'_n, of $\mathbf{E}^{(i)}$ for a given Principal Component, $\mathbf{PC}^{(i)}$. Four of the spectra, each of which forms a column of the Jacobian $J_{\nu,n} = \frac{\partial \bar{I}_\nu}{\partial p_n}$, are shown in figure A1. These spectra, and the others that are not shown here, are not orthonormal, so linear regression is necessary to determine what atmospheric variations are responsible for the spectral variability. This is done in two parts: Stepwise Regression (SR; Draper and Smith, 1981) is used to determine and to remove the cloud contribution, and Singular Value Decomposition (SVD) is used to determine the contributions of other parameters. SR correlates each cloud spectrum in the Jacobian with the Principal Component $\mathbf{PC}^{(i)}$ and subtracts those contributions from the Principal Component which are judged to be significant by partial-f-testing. After the effect of cloud is removed from the Principal Component, a new 15-element Principal Component, $\widetilde{\mathbf{PC}}^{(i)}$ remains. It may seem that the adjusted Principal Component derived here should be nearly the same as a Principal Component derived from screened (clear-sky) data; however, temperature and humidity correlate strongly with cloud cover, and the two Principal Components can differ.

SVD solves for the temperature and humidity components of the atmospheric profile which fit $\widetilde{\mathbf{PC}}^{(i)}$ best in the least-χ^2 sense. In SVD, the reduced Jacobian, $\tilde{\mathbf{J}}$, is decomposed into orthonormal vector bases by

$$\tilde{\mathbf{J}} = \mathbf{Y}\Lambda\mathbf{V}^{\mathrm{T}}, \tag{A1}$$

in which the T-superscript denotes a matrix transpose, the columns of both $\mathbf{Y}$ and $\mathbf{V}$ are orthonormal vectors, and the square matrix Λ is diagonal. The atmospheric fluctuation $\tilde{\mathbf{E}}^{(i)}$ related to each adjusted Principal Component $\widetilde{\mathbf{PC}}^{(i)}$ is then given by

$$\tilde{\mathbf{E}}^{(i)} = \mathbf{V}\Lambda^{-1}\mathbf{Y}^{T}\,\widetilde{\mathbf{PC}}^{(i)}. \tag{A2}$$

Each element of the vector $\tilde{\mathbf{E}}^{(i)}$ can generate a contribution to the adjusted Principal Component, and each one of these expansions thus represents part of the variability represented by the observed spectral variability. For example, Table 4 lists these contributions given the first Principal Component from the ensemble of all Amazon spectra.

It is unnecessary to use all of the diagonal elements of Λ in the evaluation of equation (A2). The higher order elements contain little explained variance (c.f. table A1). If the higher order components of Λ are omitted, the inversion becomes more stable at the expense of averaging between elements. This is one of the advantages of SVD -- that it enables its user to eliminate "nullity" in the Jacobian. Trial and error indicated that 13 elements of Λ (and columns of $\mathbf{Y}$ and $\mathbf{V}$) are appropriate for the conditions in the tropical oceans, but that 11 are better for the more disturbed conditions in mid-latitudes. Figure A2 shows retrievals for the Warm Pool for 12, 13, and 14 eigenvalues; 12 eigenvalues are judged to average too severely above 6 km, and the similarities between the retrievals for 13 and 14 eigenvalues indicates that both were stable.

References

Bell, T.L., 1980: Climate sensitivity from fluctuation dissipation: Some simple model tests. *J. Atmos Sci.*, **37**, 1701-1707.

Bernstein, L. S., A. Berk, P.K. Acharya, D.C. Robertson, G.P. Anderson, J.H. Chetwynd, and L.M. Kimball, 1996: Very Narrow Band Model Calculations of Atmospheric Fluxes and Cooling Rates Using the MODTRAN Code. *J. Atmos. Sci.*, **53**, 2887-2904 .

Draper, N.R. and H. Smith, 1981: *Applied Regression Analysis* . Wiley and Sons, 709 pp.

Derber, J., 1989: A variational continuous assimilation technique. *Mon. Wea. Rev.*, **117**, 2437-2446.

Errico, R.M. and T. Vukicevic, 1992: Sensitivity Analysis Using an Adjoint of the PSU-NCAR Mesoscale Model. *Mon. Wea. Rev.*, **120**, 1644-1660.

Gates, W.L., A. Henderson-Sellers, G.J. Boer, C.K. Folland, A. Kitch, B.J. McAveney, F Semazzi, N. Smith, A.J. Weaver, and Q.-C. Zeng, 1996: Climate Models - validation. *Climate Change 1995*, J.J. Houghton, L.G. Meiro Filho, B.A. Callander, N. Harris, A. Kattenberg, and K. Maskell, Eds. Cambridge University Press, 229 - 284.

Goody, R., and R. Haskins, 1998: Calibration of Radiances from Space. *J. Climate.*, **11**, 754-758.

Haskins, R.D., R.M. Goody, and L. Chen, 1997: A statistical method for testing a general circulation model with spectrally resolved data. *J. Geophys. Res.*, **102**, 16,563-16,581.

Kim, K.-Y., G. North, and G. Hegerl, 1996: Comparisons of the second-moment statistics of climate models. *J. Climate*, **9**, 2204-2219.

Kneizys, F.X., E.P. Shettle, L.W. Abrue, J.H. Chetwynd, G.P. Anderson, W.O. Gallery, J.E.A. Selby, and S.A. Clough, 1988: Users guide to LOWTRAN 7. *Tech. Rep. AFGL-TR-88-0177*, Air Force Geophys. Lab., Hanscom, Mass.

Leith, C.E., 1975: Climate response and fluctuation dissipation. *J. Atmos. Sci.*, **32**, 2022-2026.

North, G.R., R.E. Bell, and J.W. Harding, 1993: Fluctuation dissipation in a general-circulation model. *Clim. Dynam.* , **8** (6), 259-264.

Polyak, I., 1996: Observed versus simulated second-moment climate statistics in GCM verification problems. *J. Atmos. Sci.*, **53**, 677-694.

Polyak, I., and G.R. North, 1997a: Evaluation of the Geophysical Fluid Dynamic Laboratory General-Circulation Model climate variability Part 1: Variances and zonal time-series. *J. Geophys. Res.*, **102**, 1921-1929.

Polyak, I., and G.R. North, 1997b: Evaluation of the GFDL GCM climate variability Part 2: Stochastic modeling and latitude-temporal fields. *J. Geophys. Res.*, **102**, 6799-6812.

Preisendorfer, R.W., 1998: *Principal Component Analysis in Meteorology and Oceanography.* Elsevier, 512 pp.

Rodgers, C. D., 1990: Characterization and error analysis of profiles retrieved from remote sounding measurements. *J. Geophys. Res.*, **95**, 5587-5600.

Santer, B.D., and T.M.L. Wigley, 1990: Regional validation of means, variances and spatial patterns in GCM control runs. *J. Geophy. Res.*, **95**, 829-850.

Wang, J., G.P. Anderson, H.E. Revercomb, and R.O. Knuteson, 1996: Validation of FASCOD3 and MODTRAN3: comparison of model calculations with ground-based and airborne interferometer observations under clear-sky conditions. *Applied Optics*, **35**, 6028-6040.

Tables

Table 1: The geographic regions, see also figure 1. The total variances are variances with units of $(\text{radiance})^2$ summed over all frequencies. They are for 5-day averages and the complete IRIS data set, and they illustrate in a general way the regional variabilities.

Name	latitudes, deg	longitudes, deg	total variance
Warm Pool	10S to 10N	90E to 150E	8.87×10^3
Central Pacific	10S to 10N	130W to 180	3.82×10^3
Indian Ocean	10S to 10N	50E to 90E	1.26×10^4
North Pacific	45N to 60N	135W to 180	6.88×10^3
South Pacific	45S to 60S	135W to 180	5.45×10^3
Amazon	0 to 15S	65W to 48W	2.41×10^4
Sahara	10N to 30N	0 to 25N	2.24×10^4
Tundra	45N to 60N	60W to 90W	6.28×10^4

Table 2: Jacobian elements that have correlation coefficients of 0.9 or higher.

W2	with	C4,T2
W4	with	T4
W8	with	T6
T0	with	C4,T2
T30	with	T40
C8,C12,C16	with	C8,C12,C16

Table 3: *Contribution rms* from SR/SVD analysis of PC1 and PC2 for North and South Pacific data. 1-day and 15-day averages are compared. Only the two most important non-cloud elements are given. Calculations were made with elements based on both summer and winter standard atmospheres. *Contribution rms*'s are shown in parentheses (summer followed by winter).

		1-day				15-day	
	PC1		PC2		PC1		PC2
				North Pacific			
	C16 (3.39-31.4)		no cloud		C12(1.92-1.85)		no cloud
	T6 (0.37-0.27)		T40 (0.84-0.77)		T6 (0.55-0.33)		T40 (0.77-0.71)
	T4 (0.43-0.54)		T30 (0.33-0.29)		T4((.70-0.43)		T30 (0.27-0.24)
PC rms	3.74		1.22		2.64		1.1
g.o.f. %	99.9-99.9		99.3-99.6		99.8-99.8		99.3-99.5
				South Pacific			
	C16 (2.76-2.65)		no cloud		no cloud		C12 (2.21-2.17)
	none		T40 (0.93-0.79)		T40 (0.96-0.85)		T30 (0.38-0.39)
	none		T30 (0.83-0.89)		T30 (0.71-0.72)		T0 (0.24-0.24)
PC rms	1.92		1.87		1.61		1.87
g.o.f. %	99.9-99.9		99.5-99.6		99.4-99.6		99.8-99.8

Table 4: SR/SVD analysis for PC1 for all data in the Amazon. Only elements with *contribution rms* greater than 0.2 are listed. Significance may be judged from the relative size of the *contribution rms* and the *residual rms*. *PC rms* = 5.77; *residual rms* = 0.17; *g.o.f.* = 99.9%. Amplitudes are fractions for clouds, % relative humidity for water, and kelvin for temperature.

element	C12	W2	W8	T0	T4	T6	T12
amplitude	+0.09	+14%	41%	-0.86K	0.80K	-1.9K	-3.7K
contribution rms	5.62	0.51	0.45	0.42	0.48	0.34	0.34

Table 5: Total variances (see Table 1 for definition) for the Sahara, by averaging time and by season.

all data, by averaging time		5-day averages, by season	
1-day	3.91×10^4	djf	0.65×10^4
2-day	2.78×10^4	mam	3.03×10^4
5-day	2.24×10^4	jja	1.53×10^4
15-day	0.99×10^4	son	0.72×10^4

Table 6: SR/SVD analysis of PC1 for all data from the Sahara with 5-day averages. Only significant and consistent elements are listed. W2 was significant but inconsistent. Analysis was performed using both summer and winter elements and both values are given.

	summer	winter
cloud	no cloud	no cloud
T0 amplitude, K	+3.7	+4.3
T0 contribution rms	3.44	5.99
C4T2 amplitude, K	+2.2	+3.8
C4T2 contribution rms	1.82	2.09
PC rms	3.72	3.72
residual rms	0.33	0.39
g.o.f.	99.2	98.9

Table 7: Total variances (see Table 1 for definition) for the Siberian Tundra, by averaging time and by season.

1-day	7.10 x 10^4	djf	0.36 x 10^4
2-day	6.81 x 104	mam	1.96 x 10^4
5-day	6.28 x 10^4	jja	1.03 x 10^4
15-day	5.52 x 10^4	son	4.76 x 10^4

Table 8: SR/SVD analysis of PC1 for all data, 5-day averages, for the Siberian Tundra. Analyses were made with both summer and winter elements; both results are shown. The only elements listed are both significant and consistent.

	summer	winter
cloud	no cloud	no cloud
T0 amplitude, K	+5.1	+5.1
T0 contribution rms	3.1	5.01
C4T2 amplitude, K	+3.5	+6.3
C4T2 contribution rms	3.09	5.01
T4 amplitude, K	+5.7	+11.7
T4 contribution rms	2.75	1.97
T6 amplitude, K	+11.2	+6.2
T6 contribution rms	1.75	0.67
T40 amplitude, K	+6.8	+7.9
T40 contribution rms	0.52	0.48
PC rms	4.55	4.55
residual rms	0.32	0.27
g.o.f.	99.51	99.65

Table A1: Eigenvalues and explained variance for an SVD expansion of tropical, non-cloud elements.

number	eigenvalue	explained variance (%)
1	67.33	27.25
2	53.28	21.56
3	30.42	12.31
4	24.18	9.78
5	20.63	8.35
6	14.94	6.05
7	11.77	4.76
8	8.23	3.33
9	4.97	2.01
10	4.11	1.66
11	3.32	1.34
12	1.74	0.71
13	1.16	0.47
14	0.75	0.30
15	0.29	0.12

Figure Captions

Figure 1: The geographic regions, see also table 1.

Figure 2: IRIS observations in the Central Pacific region for a 5-day period, from mission day 117 to 121. The filled ellipse at the lower left indicates the IRIS footprint. Crosses are for local noon equator crossings and circles for local midnight crossings. The lines indicate the GCM grid. GCM data at 0 and 12 GMT were used.

Figure 3: Retrievals for the Warm Pool, 5-day averages, all data: a. PC1; b. residual (PC1-best fit PC from SR/SVD inversion). Note the unsatisfactory fit for the CO_2 Q-branches at 618 and 721 cm^{-1}.

Figure 4: IRIS data for the Warm Pool. "all data" refers to the entire IRIS data set (5527 spectra recorded over 10 months), while "screened" refers to the clear-sky data (597 spectra). E.V. is the explained variance of the PC. 5-day averages are employed: a. average radiances; b. standard deviations; c. PC1s; d. PC2s.

Figure 5: IRIS data for the Central Pacific. Details as for figure 4. "all data" involves 9872 spectra, while "screened" involves 5006.

Figure 6: IRIS data for the Indian Ocean. Details as for figure 4. "all data" involves 7979 spectra, while "screened" involves 2089.

Figure 7: The vertical structure of covariance of PC1s (see figures 4, 5, and 6) for the complete data set for: a. the Central Pacific; b. Warm Pool; c. Indian Ocean. The contributions (left of each pair)

are from the SVD solution (see Appendix). The lowest 0.5 km is assigned to T0. The right member of each pair shows the associated *contribution rms* (clear areas) and the *residual rms* (shaded area). The test of significance is whether a *contribution rms* exceeds the *residual rms*. Data on the cloud from the SR solution and other rms data are given below.

	Central Pacific	Warm Pool	Indian Ocean
PC rms	2.30	3.49	4.16
cloud height, km	16	12	16
cloud rms	1.63	3.38	4.11
residual rms	0.09	0.09	0.12
g.o.f. %	99.85	99.93	99.92

Figure 8: Comparison between PC1s, 5-day averages, for Central Pacific: a. PC1s; b. SR/SVD analysis of IRIS screened (clear-sky) data; c. SR/SVD analysis of GCM data. See figure 7 for further explanation of the bottom panels. *g.o.f.* and *rms* data are shown below.

	IRIS	GCM
PC rms	0.92	0.63
residual rms	0.12	0.05
g.o.f. %	98.3	99.4

Figure 9: Comparison between PC1s, 5-day averages, for Warm Pool: a. PC1s; b. SR/SVD analysis of IRIS screened (clear-sky) data; c. SR/SVD analysis of GCM data. See figure 7 for further explanation of the bottom panels. *g.o.f.* and *rms* data are shown below.

	IRIS	GCM
PC rms	0.53	0.61
residual rms	0.07	0.04
g.o.f. %	98.2	99.5

Figure 10: Comparison between PC1s, 5-day averages, for Indian Ocean: a. PC1s; b. SR/SVD analysis of IRIS screened (clear-sky) data; c. SR/SVD analysis of GCM data. See figure 7 for further explanation of the bottom panels. *g.o.f.* and *rms* data are shown below.

	IRIS	GCM
PC rms	0.63	0.50
residual rms	0.09	0.03
g.o.f. %	98.0	99.6

Figure 11: Standard deviations for all data, for 1-day, 2-day, 5-day and 15-day averages: a. North Pacific; b. South Pacific; c. Central Pacific

Figure 12: PC1 for all data, 1-day and 15-day averages: a. North Pacific; b. South Pacific.

Figure 13: PC2 for all data, 1-day and 15-day averages: a. North Pacific; b. South Pacific.

Figure 14: IRIS data for the Amazon. 5-day averages for the complete data set are used: a. radiance; b. standard deviation; c. PC1, explained variance 97.5%; d. PC2, explained variance 1.7%.

Figure 15: IRIS data for the Sahara. 5-day averages are used for the complete data set: a. radiance by season; b. standard deviation; c. PC1, explained variance 93.3%; d. PC2, explained variance 5.2%.

Figure 16: IRIS data for the Siberian Tundra: a. radiance by season; b. standard deviation by averaging time; c. PC 1 for 5-day averages, explained variance 98.3%.

Figure A1: Four elements used in analysis. Each element represents the change in outgoing radiance when a change is made to one variable in one layer of a US Standard (tropical) Atmosphere: a. T0, 2 K change in surface temperature; b. T6, 2 K change in air temperature from 4 to 6 km; c. W2, 40% change in the relative humidity from 0 to 2 km; d. C12, unit emissivity change for a cloud with its top at 12 km.

Figure A2: Covariant amplitudes for water and temperature in the Warm Pool from SR/SVD retrievals 5-day averages for all data: a. 14 eigenvalues; b. 13 eigenvalues; c. 12 eigenvalues.

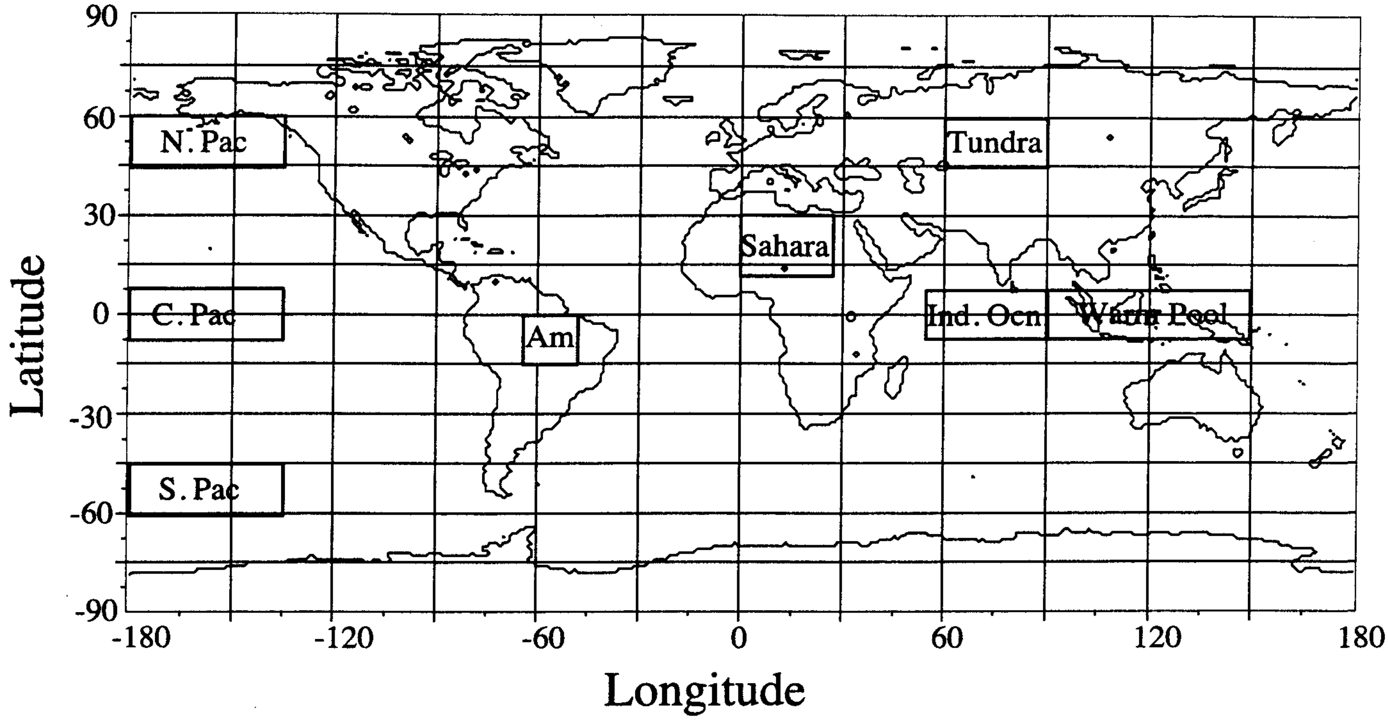

90
60
30
0
-30
-60
-90
Latitude
-180
-120
-60
0
60
120
180
Longitude
N. Pac
C. Pac
S. Pac
Am
Sahara
Tundra
Ind. Ocn
Warm Pool

fig. 1

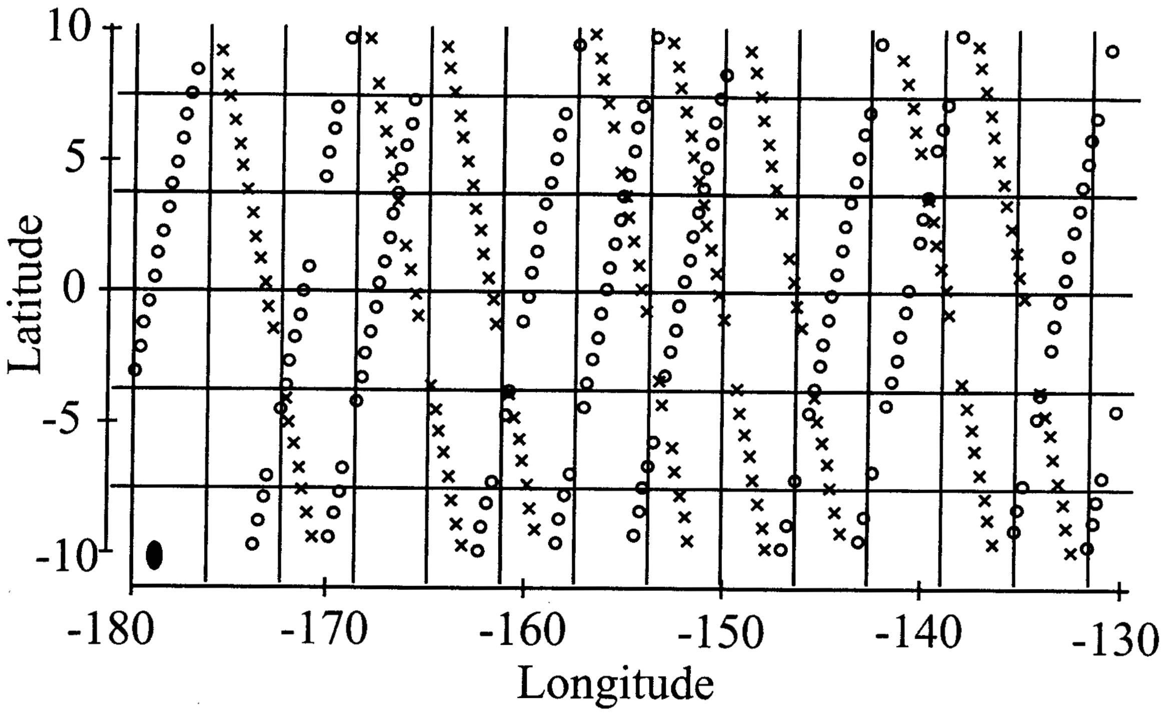

fig. 2

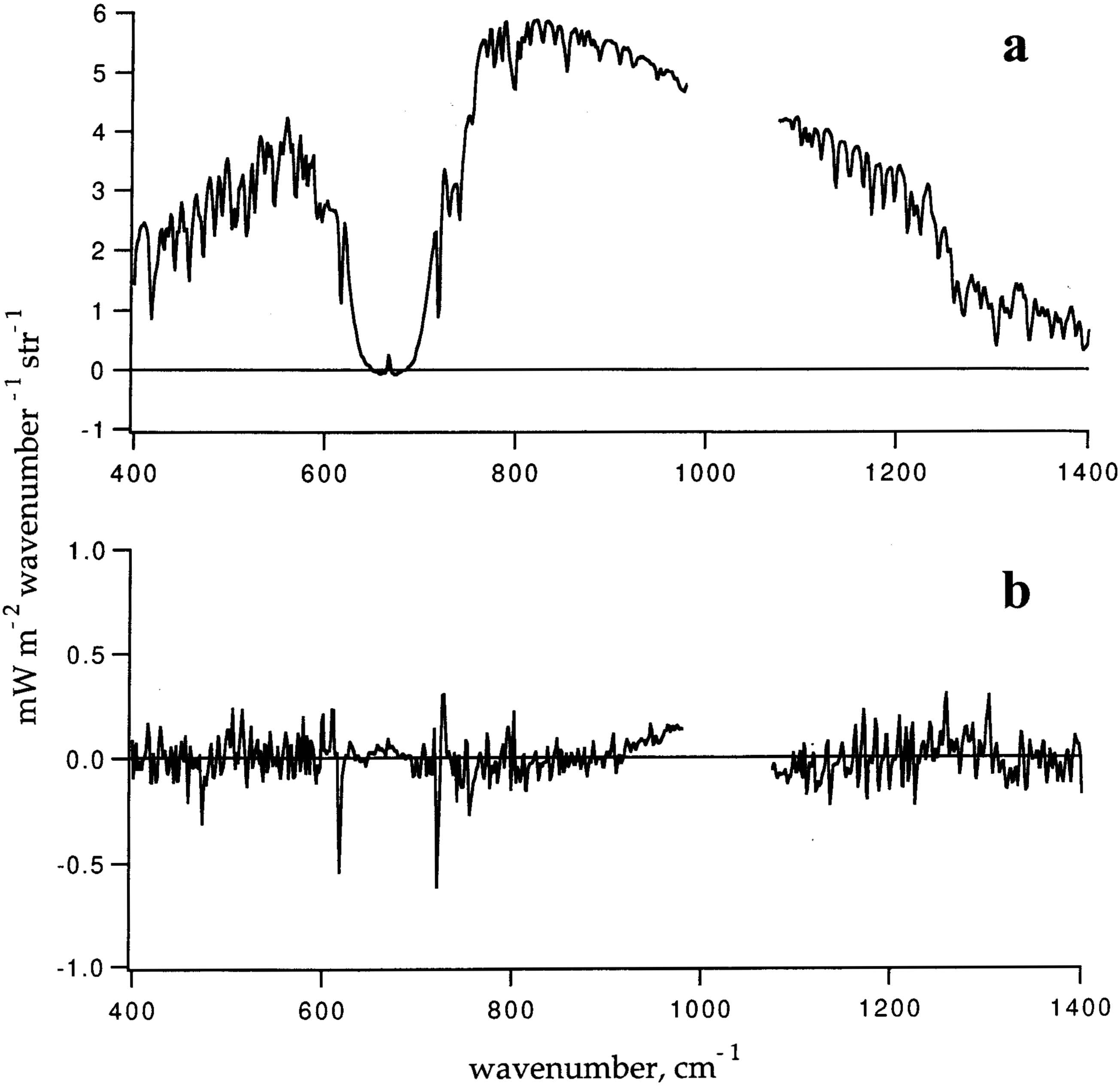
a
b
mW m^{-2} wavenumber^{-1} str^{-1}
wavenumber, cm^{-1}
6
5
4
3
2
1
0
-1
1.0
0.5
0.0
-0.5
-1.0
400
600
800
1000
1200
1400

fig.3

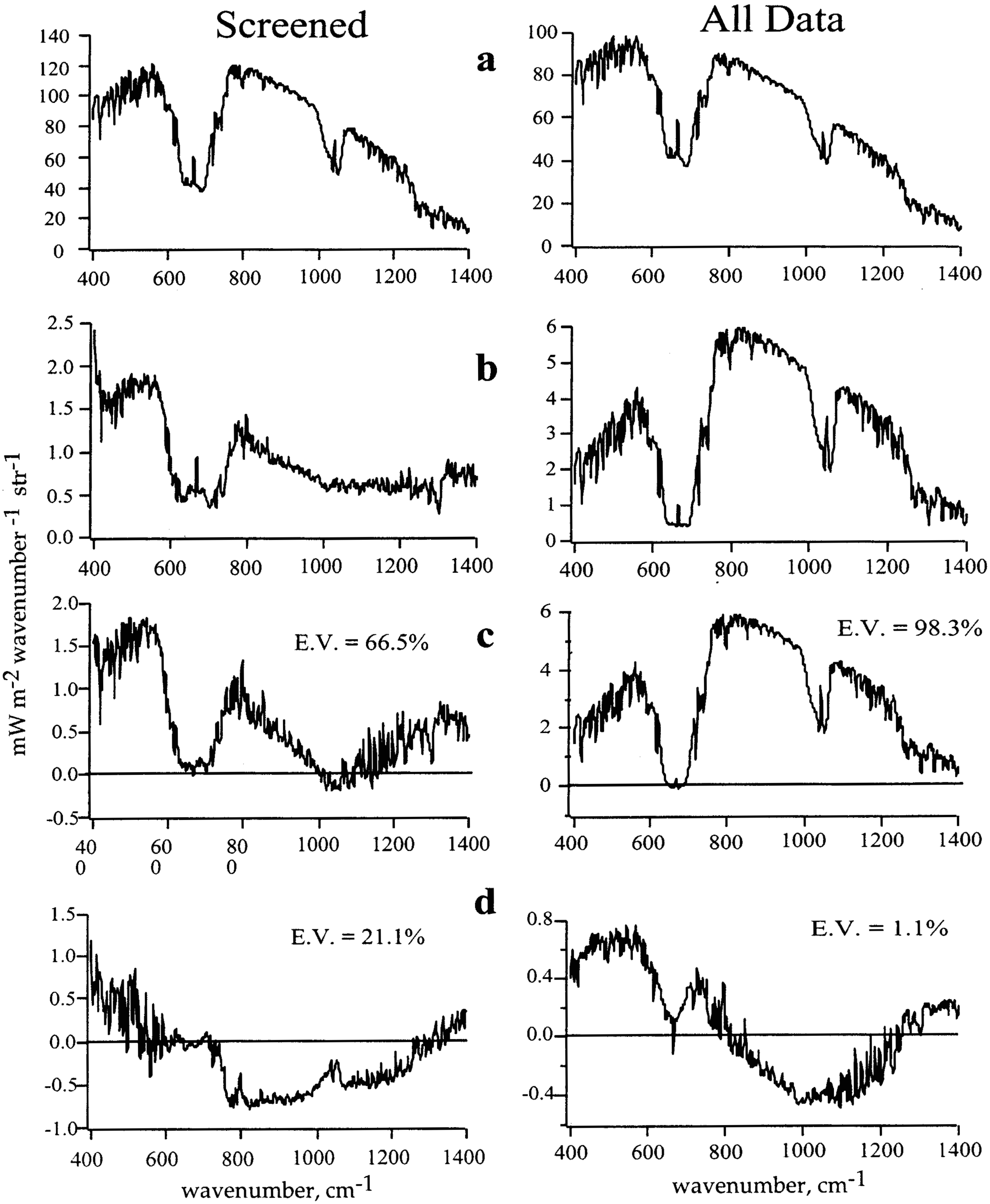
Screened
All Data
a
b
c
d
E.V. = 66.5%
E.V. = 98.3%
E.V. = 21.1%
E.V. = 1.1%
mW m-2 wavenumber -1 str-1
wavenumber, cm-1
wavenumber, cm-1

fig 4

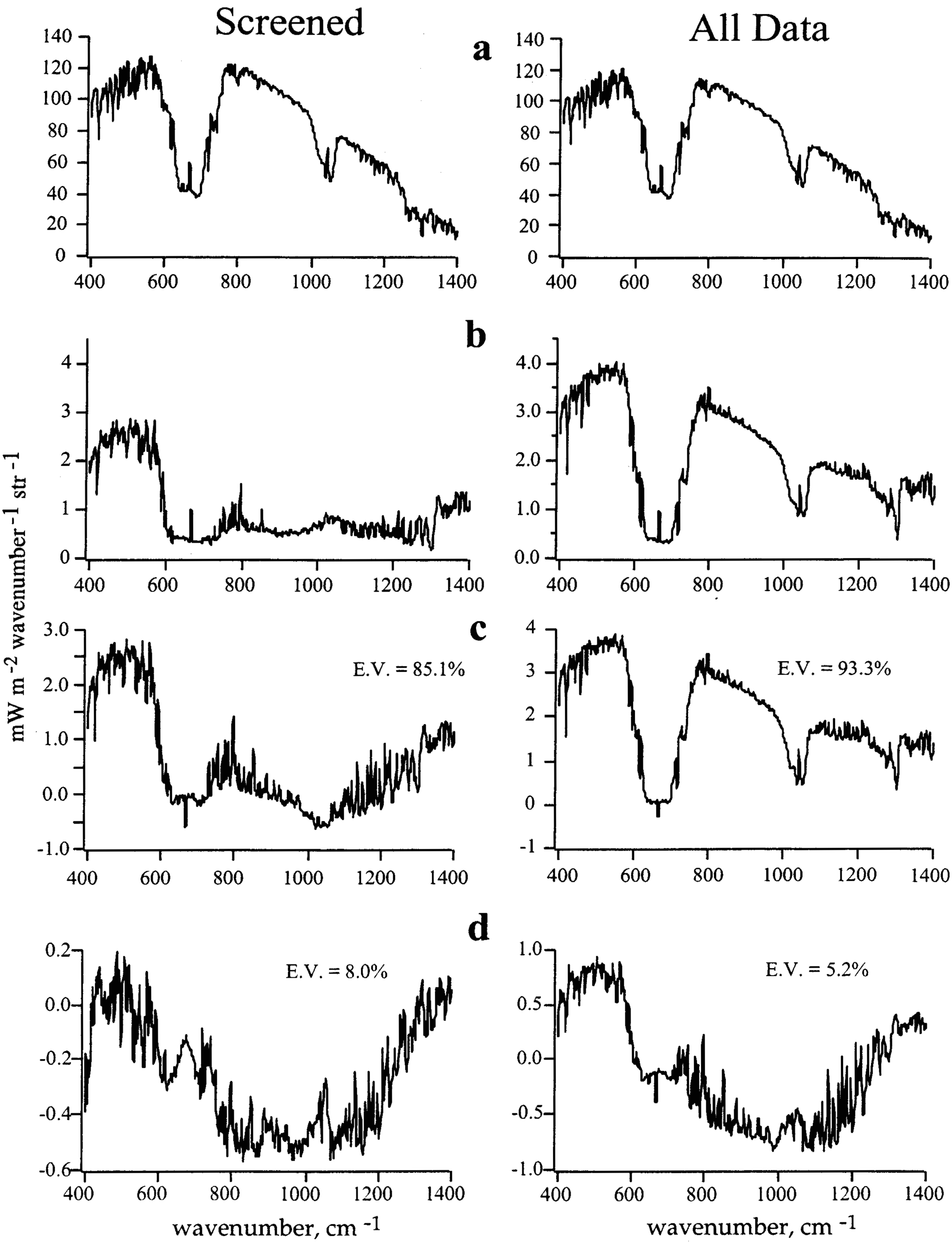
Screened
All Data
a
b
c
d
E.V. = 85.1%
E.V. = 93.3%
E.V. = 8.0%
E.V. = 5.2%
mW m -2 wavenumber -1 str -1
wavenumber, cm -1
wavenumber, cm -1

fig. 5

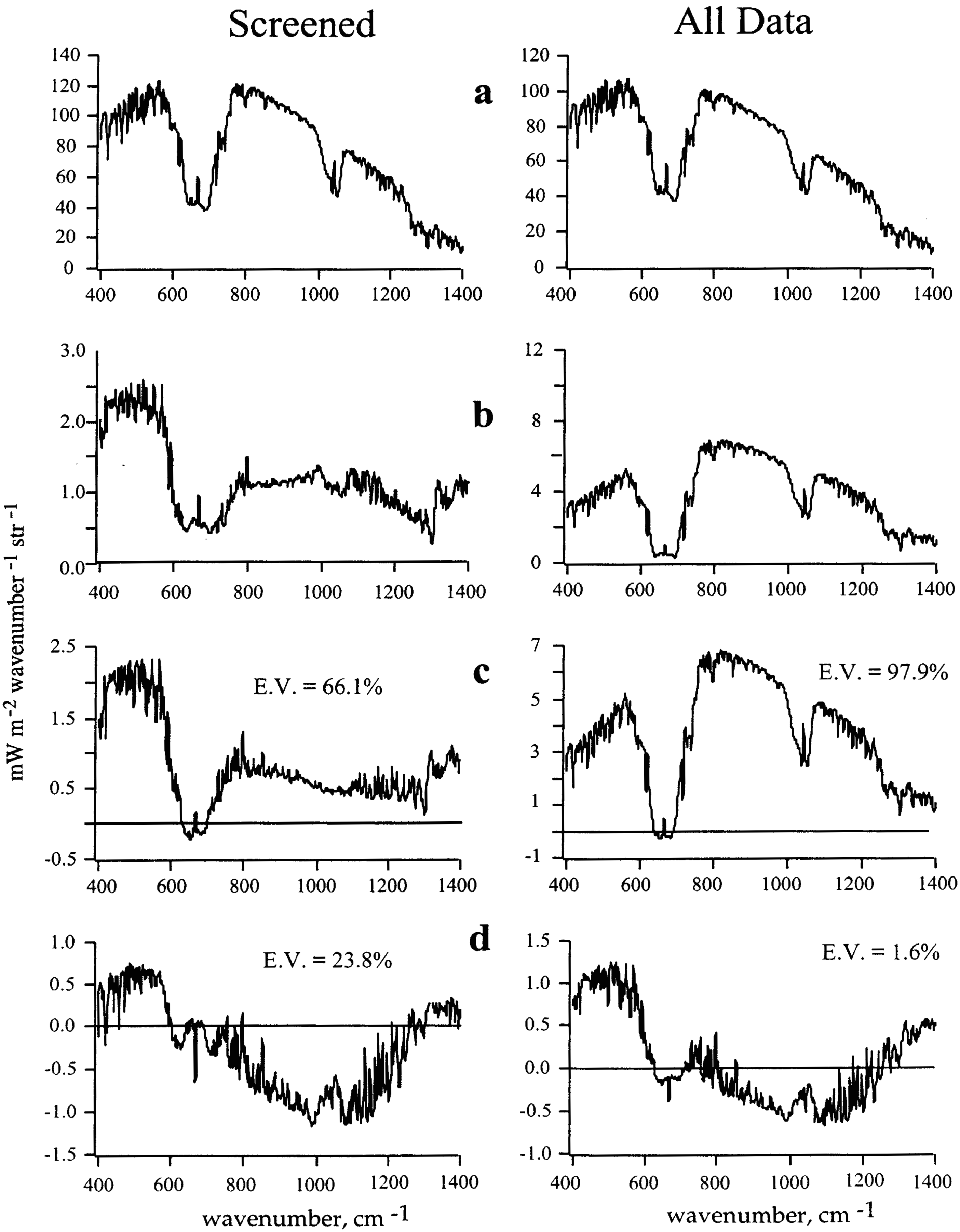
Screened
All Data
a
b
c
d
E.V. = 66.1%
E.V. = 97.9%
E.V. = 23.8%
E.V. = 1.6%
mW m-2 wavenumber -1 str -1
wavenumber, cm -1
wavenumber, cm -1

fig. 6

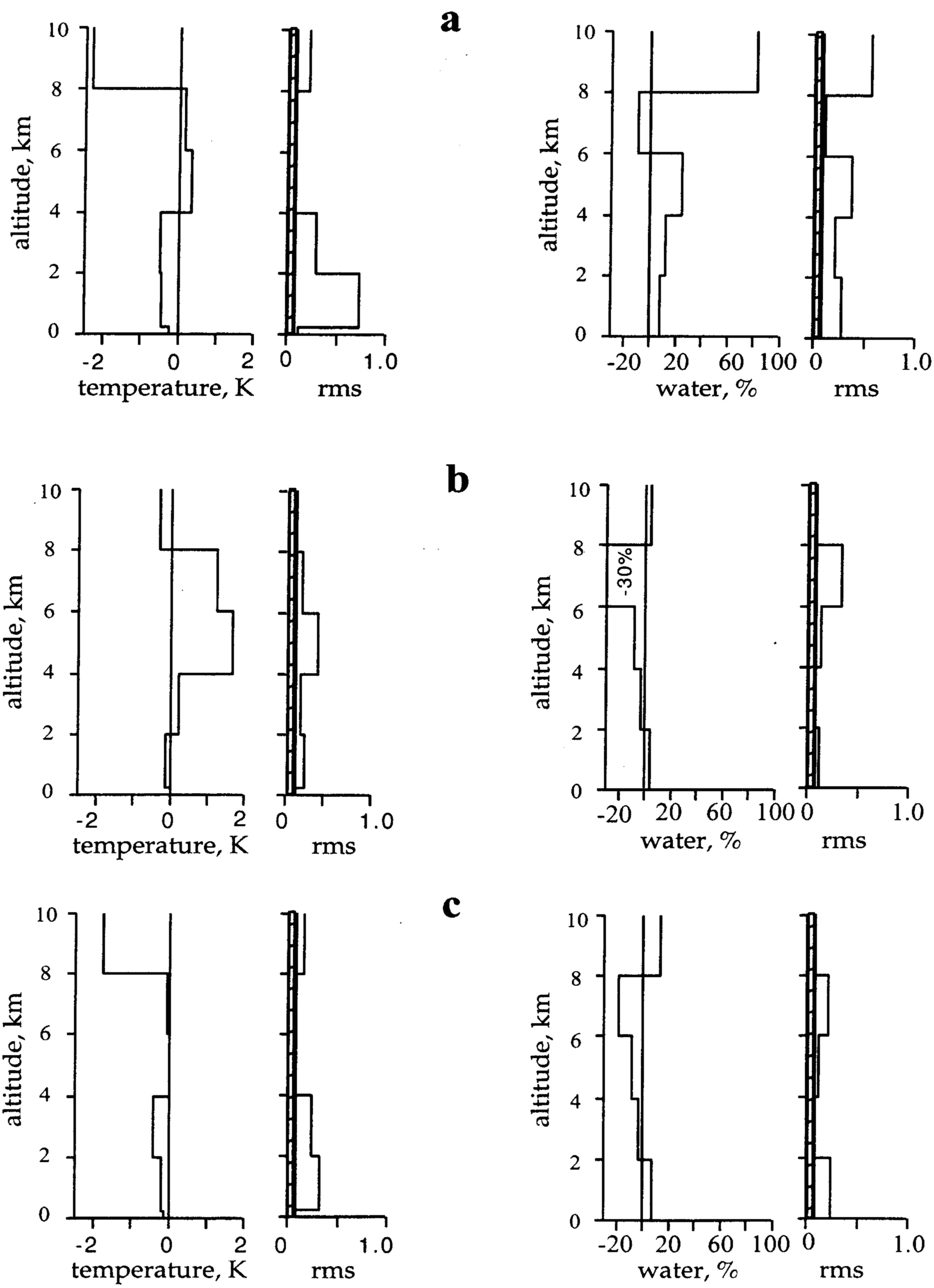
a
b
c
altitude, km
temperature, K
rms
water, %
-30%
10
8
6
4
2
0
-2
0
2
1.0
-20
20
60
100

fig. 7

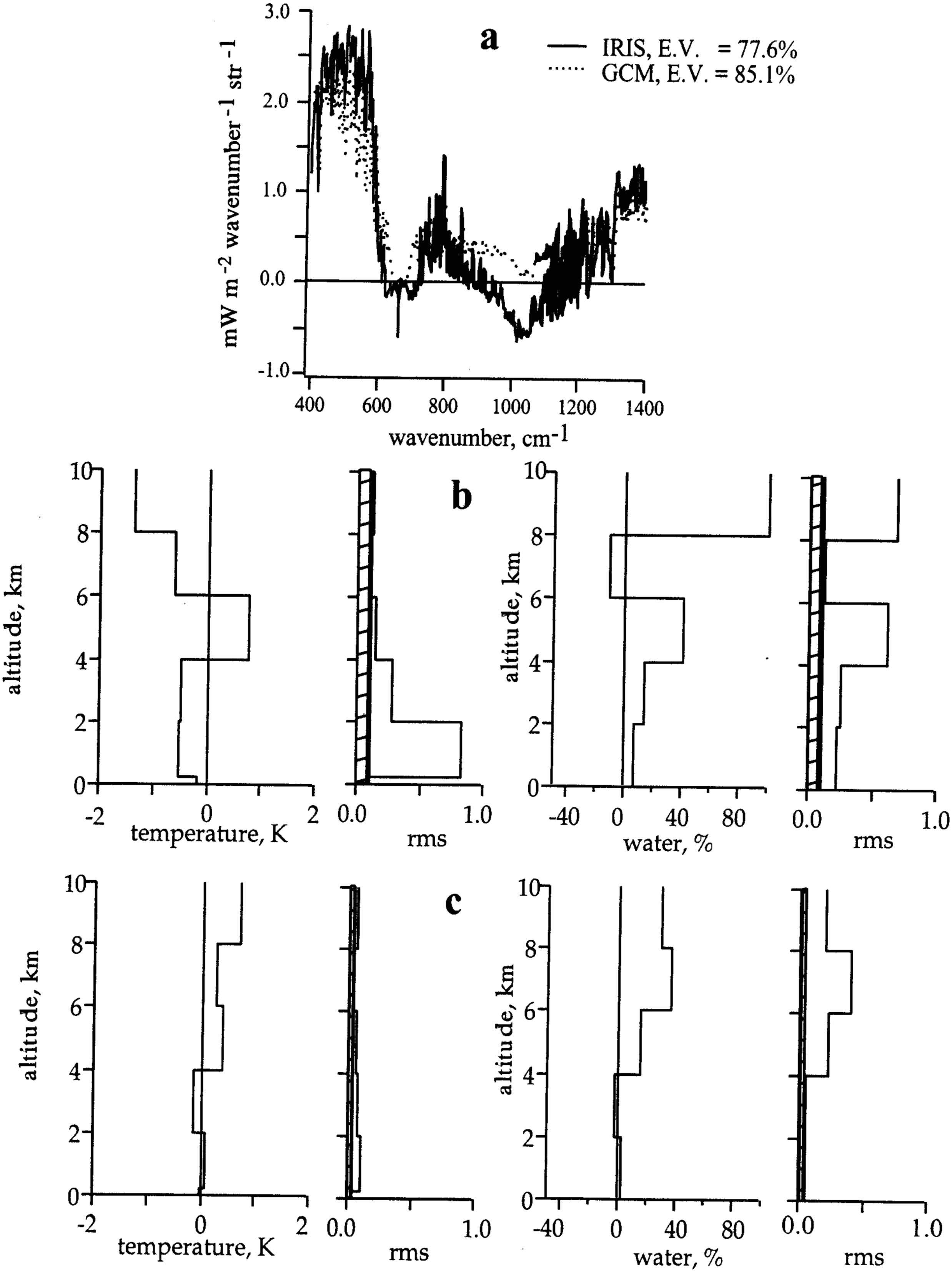
a
IRIS, E.V. = 77.6%
GCM, E.V. = 85.1%
mW m -2 wavenumber -1 str -1
wavenumber, cm-1
b
c
altitude, km
temperature, K
rms
water, %

fig 8

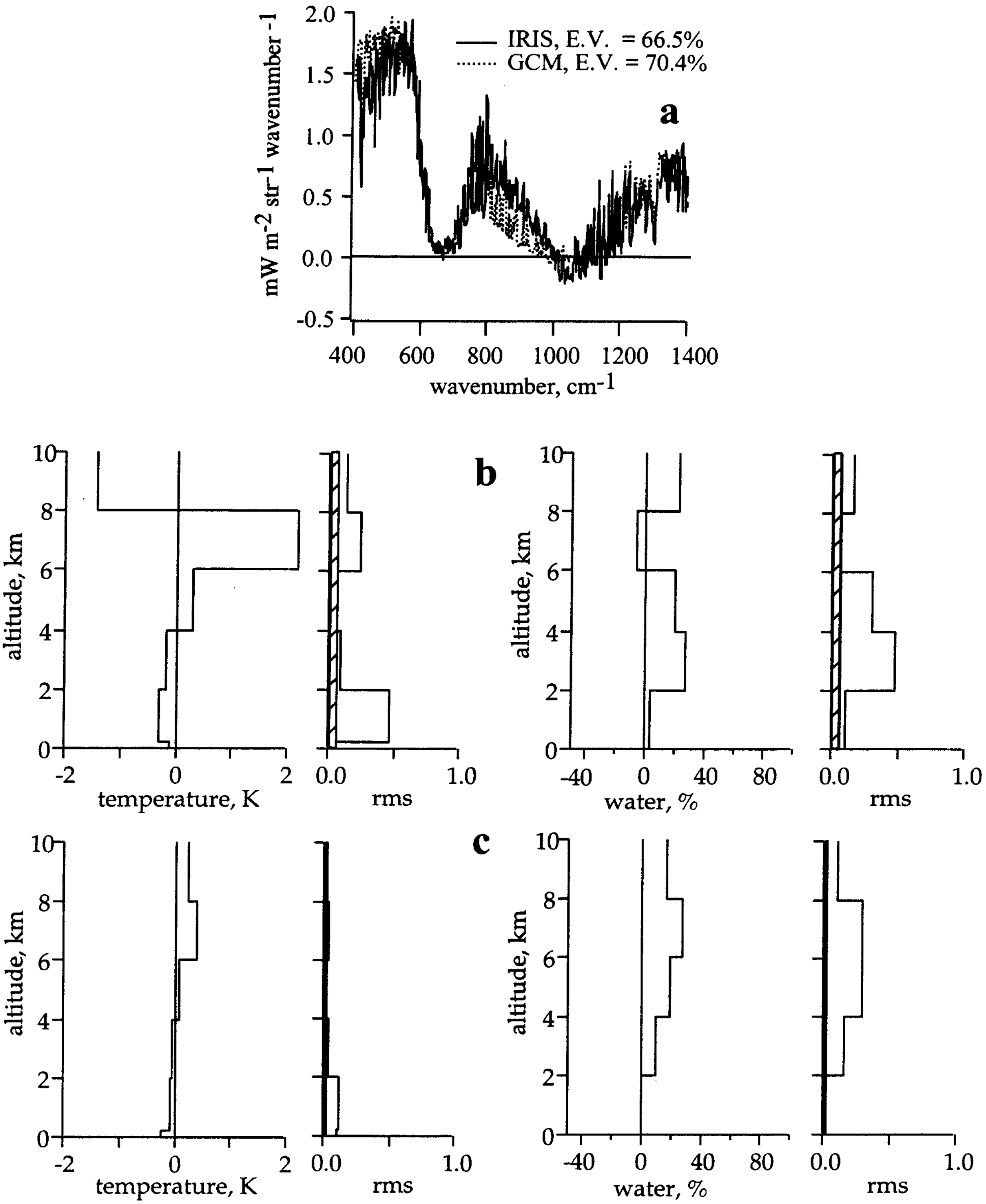
IRIS, E.V. = 66.5%
GCM, E.V. = 70.4%
a
mW m-2 str-1 wavenumber -1
wavenumber, cm-1
b
c
altitude, km
temperature, K
rms
water, %

fig. 9

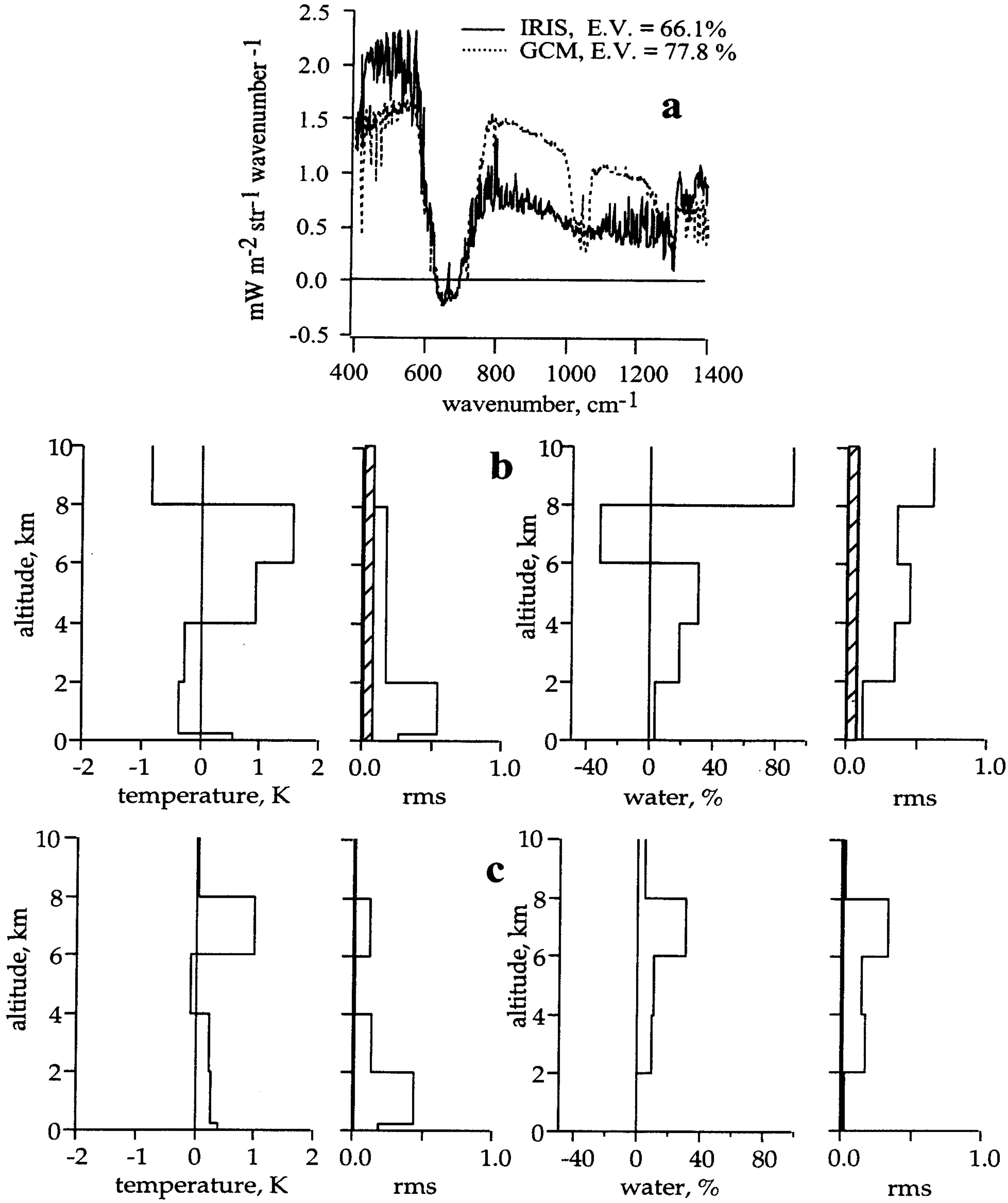
IRIS, E.V. = 66.1%
GCM, E.V. = 77.8 %
a
mW m-2 str-1 wavenumber -1
wavenumber, cm-1
b
c
altitude, km
temperature, K
rms
water, %

fig. 10

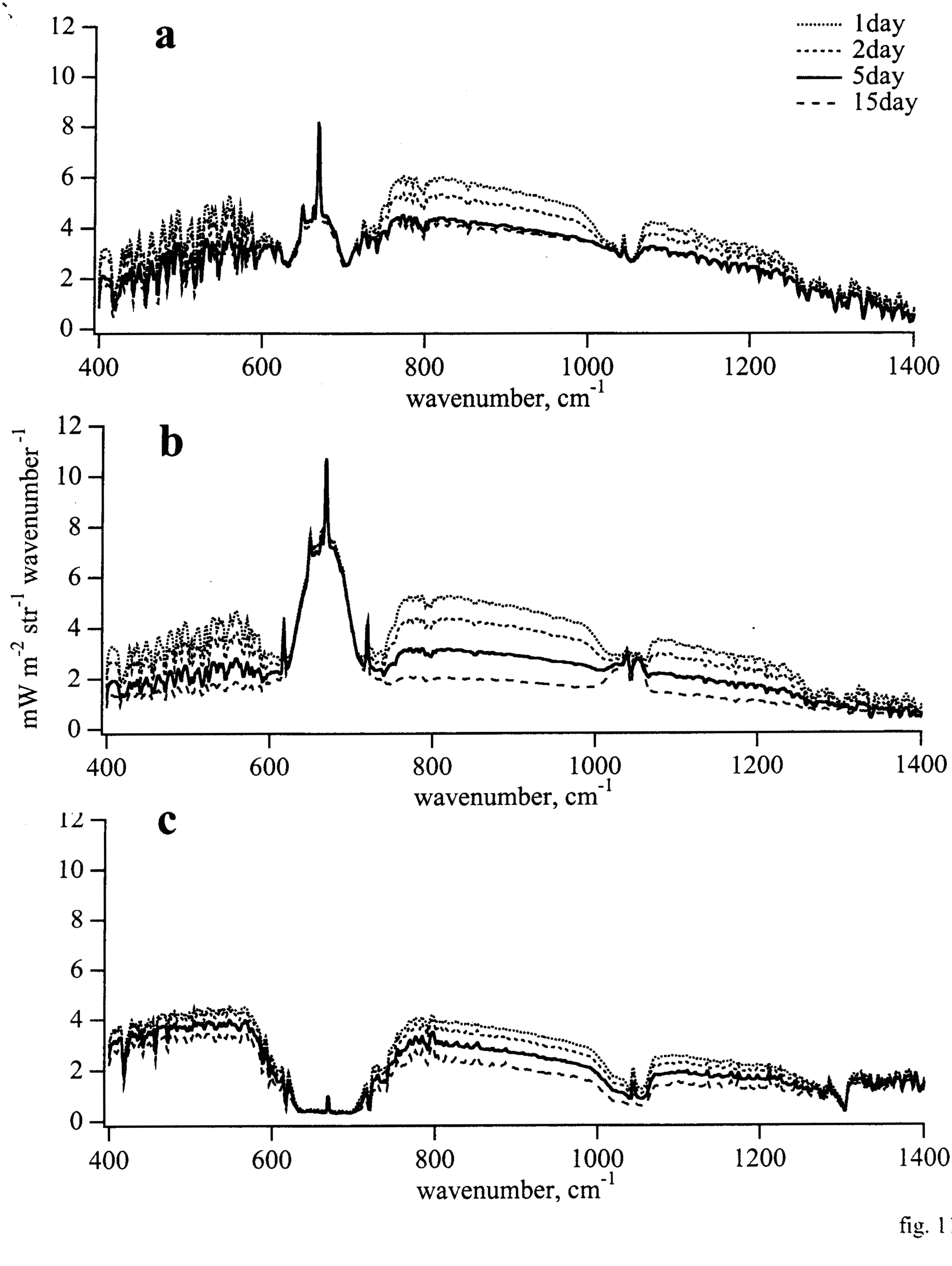

1day
2day
5day
15day
a
b
c
mW m^{-2} str^{-1} wavenumber^{-1}
wavenumber, cm^{-1}
0
2
4
6
8
10
12
400
600
800
1000
1200
1400

fig. 11

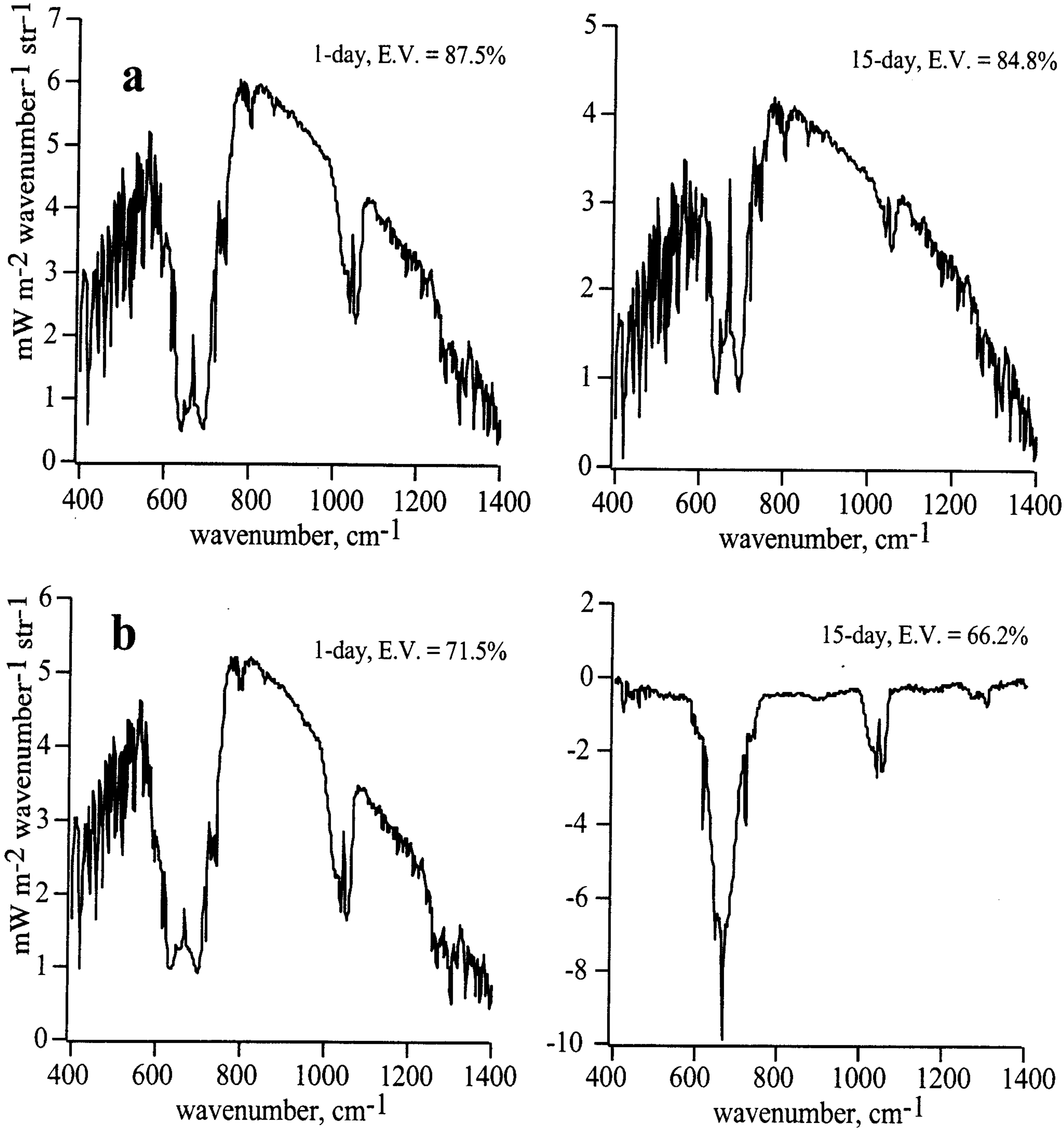

a
1-day, E.V. = 87.5%
15-day, E.V. = 84.8%
b
1-day, E.V. = 71.5%
15-day, E.V. = 66.2%
mW m-2 wavenumber-1 str-1
wavenumber, cm-1

fig. 12

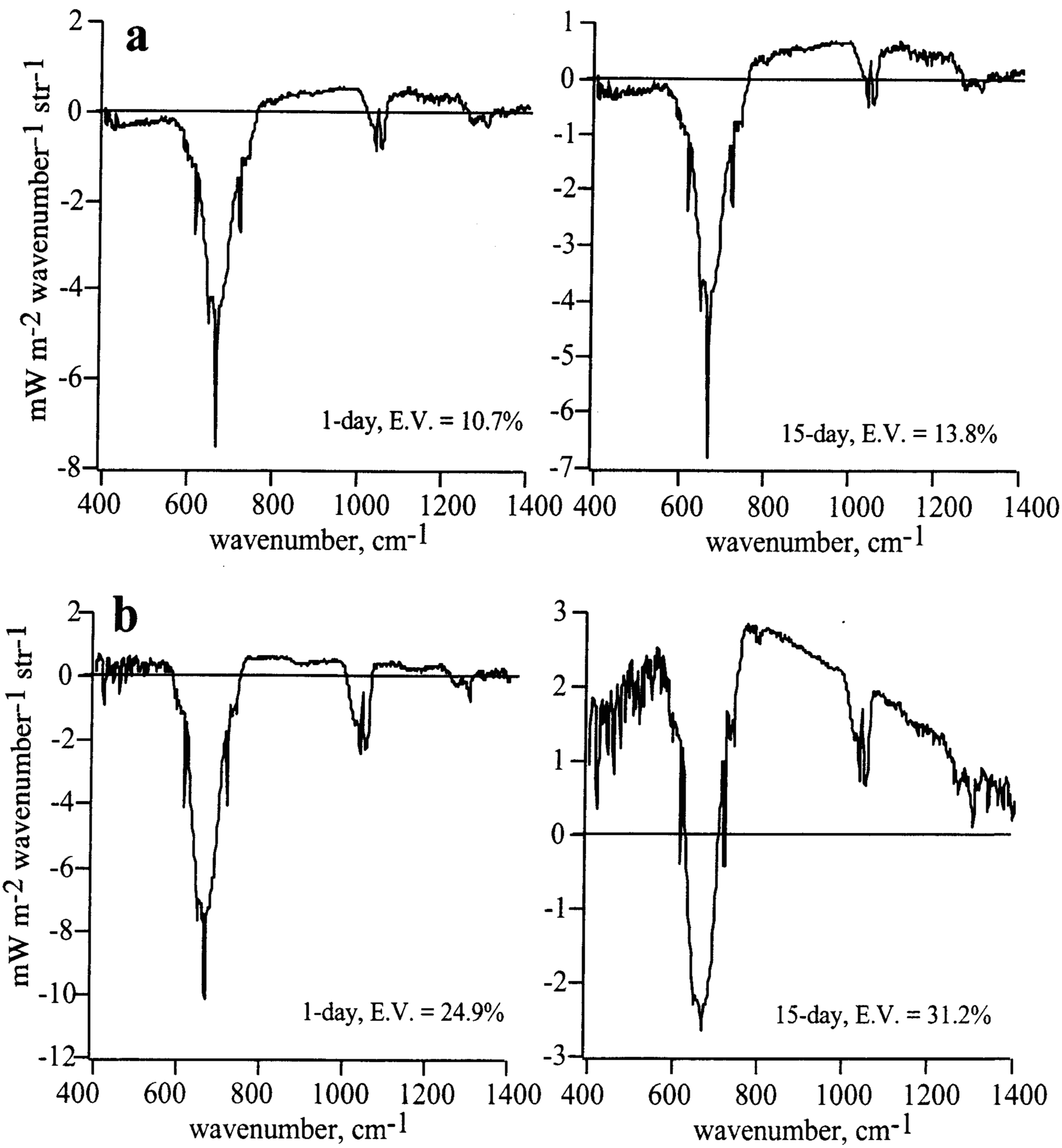
a
b
mW m-2 wavenumber-1 str-1
wavenumber, cm-1
1-day, E.V. = 10.7%
15-day, E.V. = 13.8%
1-day, E.V. = 24.9%
15-day, E.V. = 31.2%

fig. 13

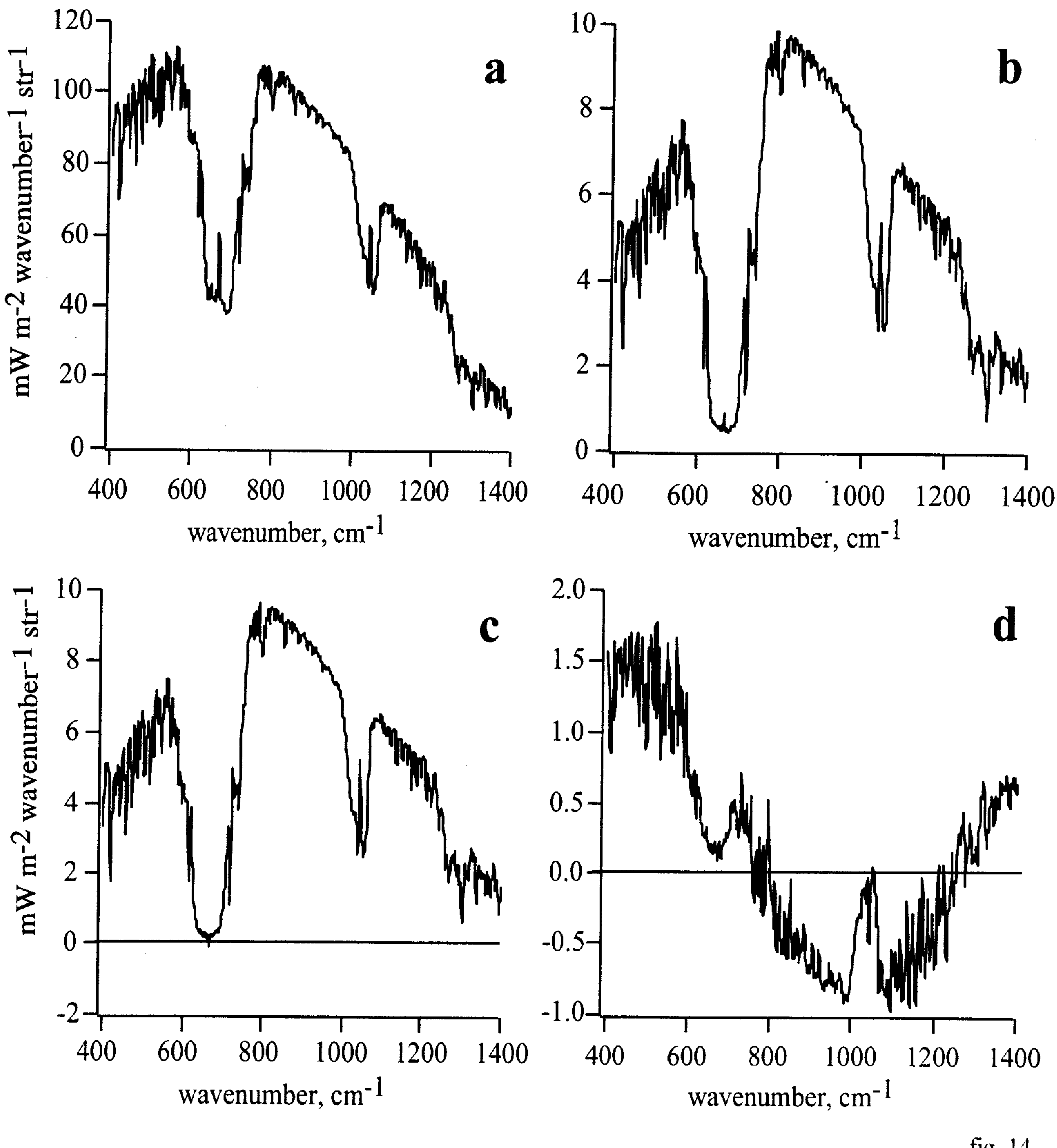

a
b
c
d
mW m-2 wavenumber-1 str-1
mW m-2 wavenumber-1 str-1
wavenumber, cm-1
wavenumber, cm-1
wavenumber, cm-1
wavenumber, cm-1

fig. 14

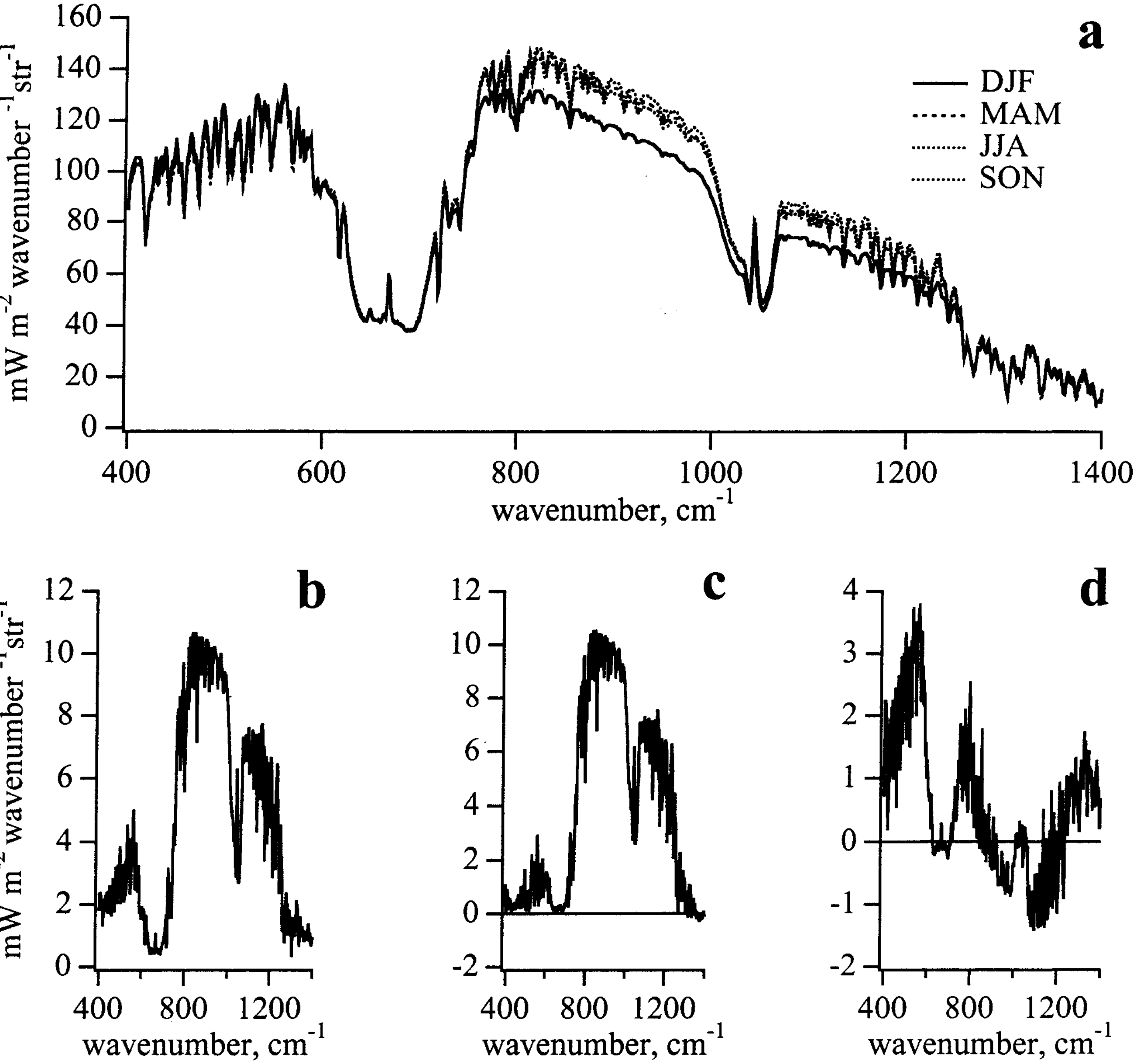

fig. 15

fig 15

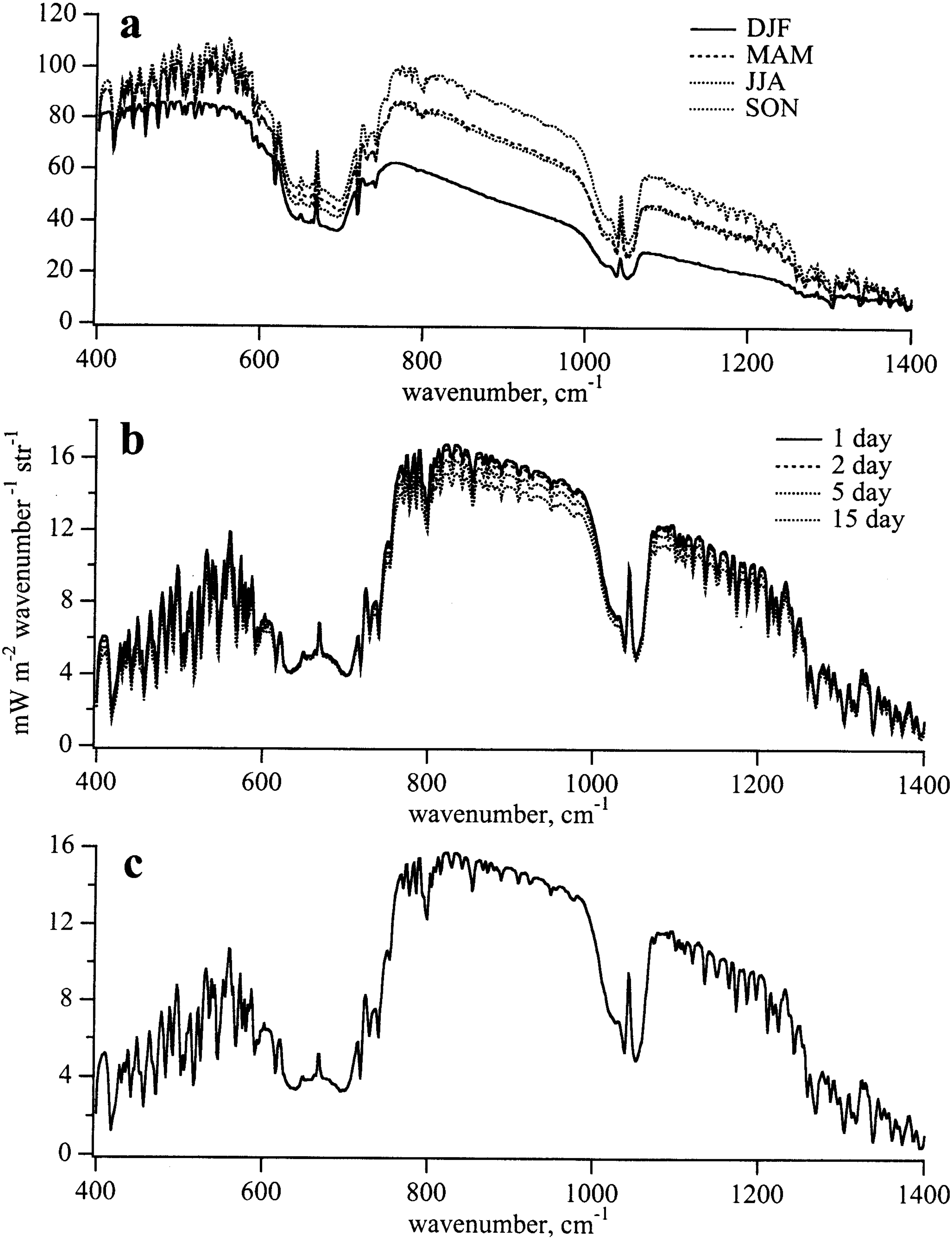
a
b
c
DJF
MAM
JJA
SON
1 day
2 day
5 day
15 day
mW m^{-2} wavenumber^{-1} str^{-1}
wavenumber, cm^{-1}
wavenumber, cm^{-1}
wavenumber, cm^{-1}
0
20
40
60
80
100
120
0
4
8
12
16
0
4
8
12
16
400
600
800
1000
1200
1400

fig. 16

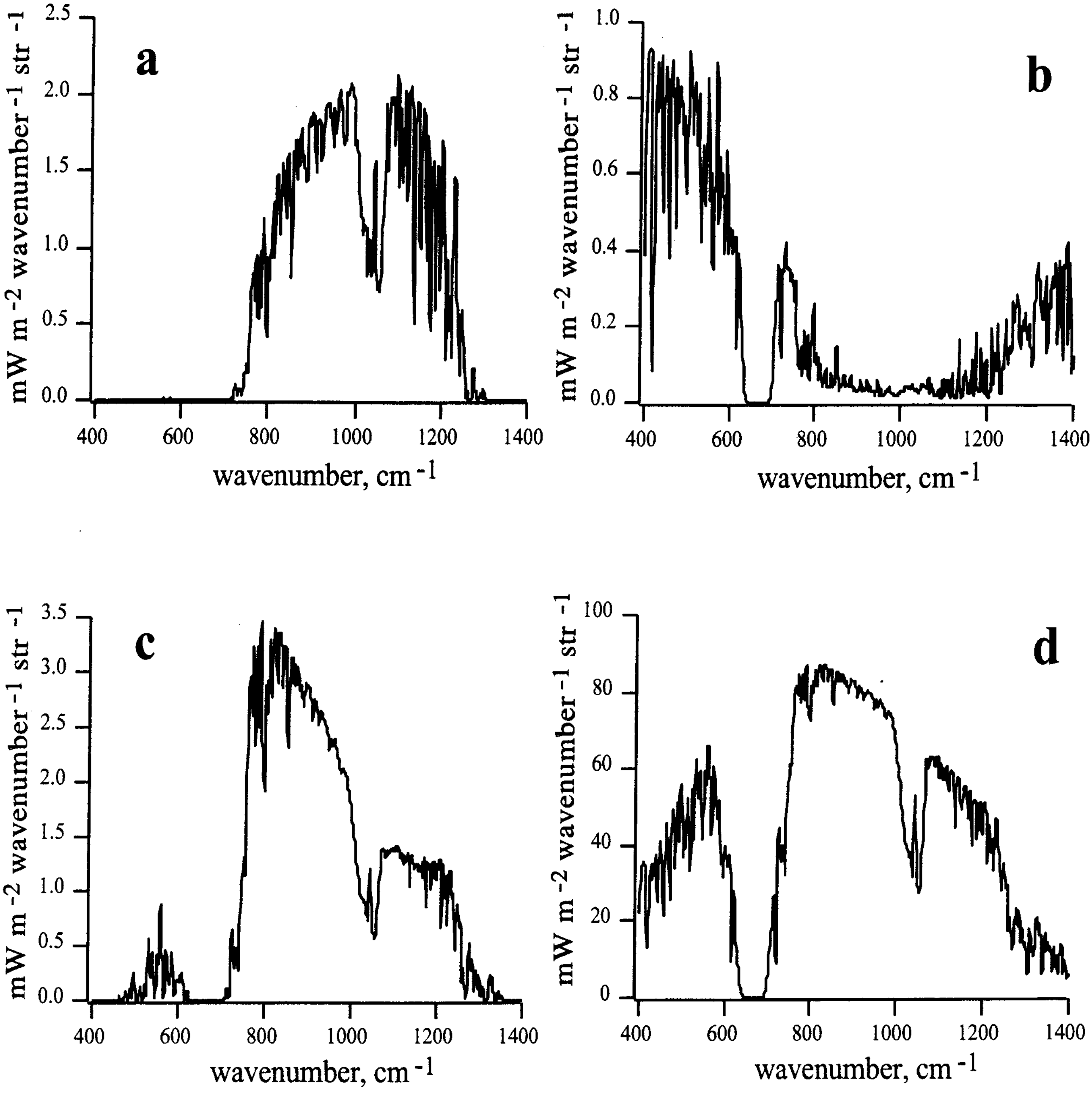

a
b
c
d
mW m -2 wavenumber -1 str -1
wavenumber, cm -1
2.5
2.0
1.5
1.0
0.5
0.0
0.8
0.6
0.4
0.2
3.5
3.0
100
80
60
40
20
0
400
600
800
1000
1200
1400

fig. A1

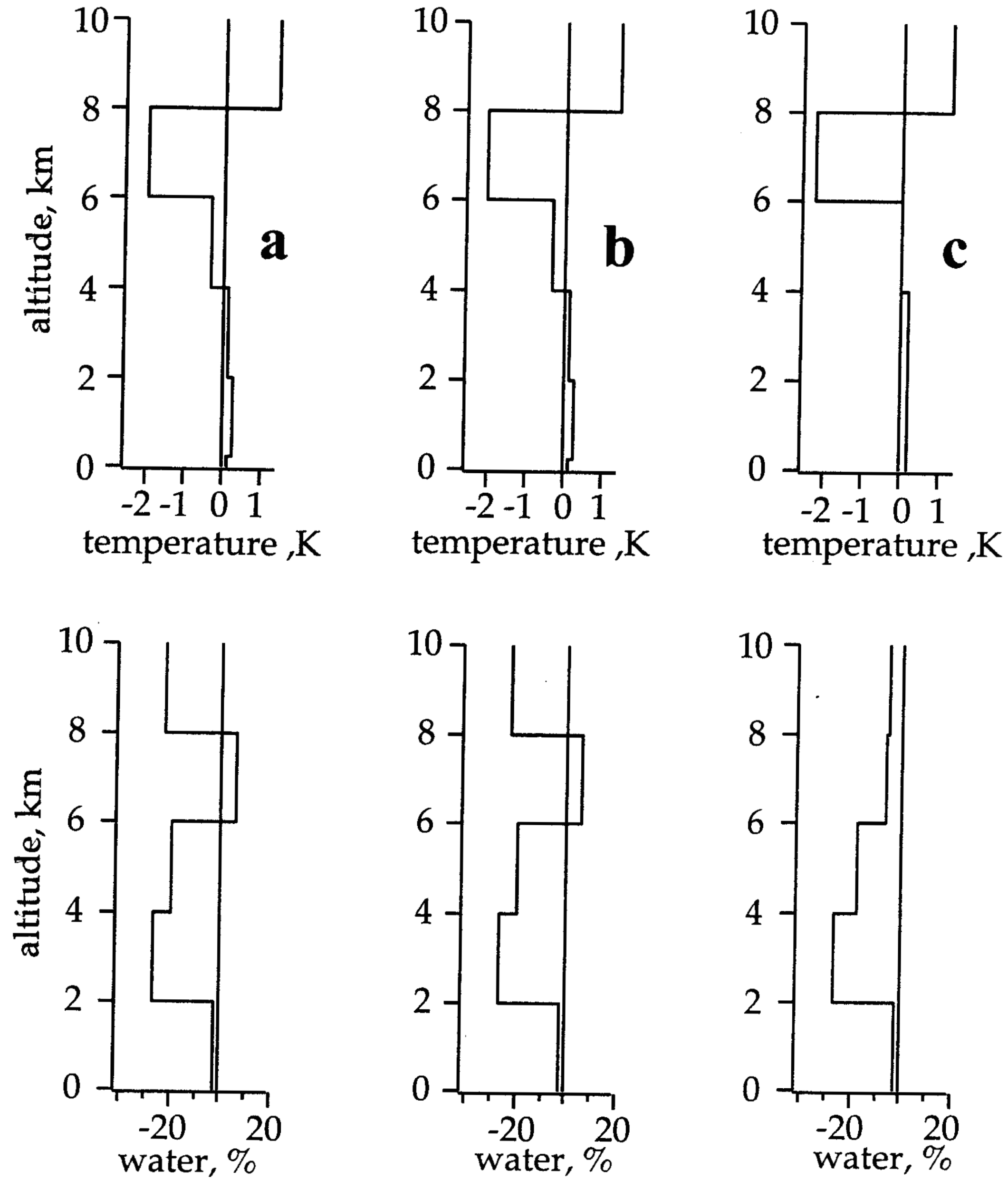

fig. A2